THE UNIVERSITY OF FLORIDA/NATIONAL CANCER INSTITUTE FAMILY OF HYBRID COMPUTATIONAL PHANTOMS REPRESENTING THE CURRENT UNITED STATES POPULATION OF MALE AND FEMALE CHILDREN AND ADOLESCENTS—APPLICATIONS TO COMPUTED TOMOGRAPHY DOSIMETRY

By

AMY M. GEYER

A THESIS PRESENTED TO THE GRADUATE SCHOOL
OF THE UNIVERSITY OF FLORIDA IN PARTIAL FULFILLMENT
OF THE REQUIREMENTS FOR THE DEGREE OF
MASTER OF SCIENCE

UNIVERSITY OF FLORIDA

2012

To my parents, who have believed in me from the day I was born

ACKNOWLEDGMENTS

I thank Dr. Wesley Bolch for the incredible opportunity he has given me to complete such meaningful research and for his guidance throughout my past academic career and my academic career yet to come. I thank Dr. Choonsik Lee for all the knowledge he has imparted to me and for the work he has done, making my research possible. I thank Dr. Lynn Rill and Dr. David Gilland for their knowledge and contribution. I thank my brother, Johnny, for paving the way. I thank my parents for their never-ending love, support, and encouragement and for always reminding me “she believed she could, so she did.”

TABLE OF CONTENTS

page

LIST OF TABLES

LIST OF FIGURES

LIST OF ABBREVIATIONS

BMI	Body mass index
CAESAR	Civilian American and European Surface Anthropometry Resource
CDC	Centers for Disease Control and Protection
CT	Computed Tomography
ICRP	International Commission on Radiological Protection
MCNPX	Monte Carlo n-particle extended
MR	Magnetic Resonance
NCI	National Cancer Institute
NCRP	National Council on Radiation Protection
NHANES	National Health and Nutrition Examination Survey
NURBS	Non-uniform B-spline surfaces
RPI	Rensselaer Polytechnic Institute
UF	University of Florida

Abstract of Thesis Presented to the Graduate School
of the University of Florida in Partial Fulfillment of the
Requirements for the Degree of Master of Science

THE UNIVERSITY OF FLORIDA/NATIONAL CANCER INSTITUTE FAMILY OF HYBRID COMPUTATIONAL PHANTOMS REPRESENTING THE CURRENT UNITED STATES POPULATION OF MALE AND FEMALE CHILDREN AND ADOLESCENTS—APPLICATIONS TO COMPUTED TOMOGRAPHY DOSIMETRY

By

Amy M. Geyer

May 2012

Chair: Wesley Bolch
Major: Biomedical Engineering

To assist in the rapid reporting of patient organ doses, researchers at the University of Florida (UF) and the National Cancer Institute (NCI) have developed a family of computational hybrid phantoms, constructed from non-uniform rational B-spline (NURBS) and polygon mesh surfaces, that fully represent the International Commission on Radiological Protection (ICRP) 89 50th percentile reference newborn, 1-year-old, 5-year-old, 10-year-old, 15-year-old male and female, and adult male and female. Coupled with Monte Carlo simulations, these phantoms can be used to estimate patient organ doses. Substantial increases seen in childhood obesity in the United States have prompted us to undergo a major revision to the UF/NCI phantom library. Furthermore, a decision was made to construct the new library in a gridded fashion by height/weight without further reference to age-dependent weight/height percentiles. At each height/weight combination, secondary circumferential parameters are also defined and used for phantom construction. All morphometric data for the new library are taken from the Centers for Disease Control and Prevention (CDC) National Health and Nutrition Examination Survey data over the time period 1999 to 2006, the most recent reported

survey period. A subset of the phantom library was then used in a computed tomography (CT) organ dose sensitivity study to examine the degree to which full Monte Carlo simulations would be required to track organ doses for patients that are severely underweight to obese in body size. Through data analysis, it was found that organ dosimetry can be established through data interpolation of a more coarsely defined voxelized phantom library subset. In the future, the UF/NCI phantom library will be used to construct pre-computed dose libraries for individuals undergoing CT examinations. Ultimately, these libraries can be deployed in the clinic for electronic recording of patient organ dosimetry following diagnostic imaging procedures.

CHAPTER 1
INTRODUCTION

With the rise in medical imaging procedures, particularly from the modalities of computed tomography (CT) and nuclear medicine, the need for accurate and detailed patient dosimetry is becoming increasingly important.[1] As established in a 2009 report by the National Council on Radiation Protection (NCRP), the effective dose per individual in the United States due to medical exposures was estimated to be 3.0 mSv.[2] This value has risen nearly six-fold from a previous per capita effective dose estimation of 0.54 mSv in 1982. Detailed computational anthropomorphic phantoms, coupled with Monte Carlo simulations, can be employed to estimate organ doses to a patient.

Computational anatomic phantoms can be classified into three format types. Stylized (mathematical) phantoms are characterized by three-dimensional geometric surface equations that define the body contour and external anatomy. Although organ repositioning and size scaling can be performed with relative ease, stylized phantoms do not provide high accuracy in dose estimates due to their simplified anatomy. Voxel phantoms represent a phantom type in which organs are defined by groups of voxels from segmented CT or magnetic resonance (MR) images. Voxel (or tomographic) phantoms provide anatomical accuracy, but offer limited flexibility when rescaling to various patient sizes. Because voxel phantoms are created from segmented CT or MR scans and from grouping voxels to define organs, these phantoms are limited by the voxel structure. In an effort to combine the flexibility of stylized phantoms with the anatomical accuracy of voxel phantoms, hybrid phantoms were developed by researchers at the University of Florida and later extended at the National Cancer Institute (NCI). Hybrid phantoms employ non-uniform rational B-spline (NURBS) and

polygon mesh (PM) surfaces that permit one to model organs with high anatomical realism while allowing ease in organ and body region deformation through the manipulation of control points (NURBS) and polygon vertices (PM) defining the surfaces of individual organ and body regions (head, arms, legs, and torso).

For each format type, phantoms can be further divided into four morphometric categories - reference, patient-dependent, patient-sculpted, and patient-specific. Reference phantoms use 50^{th}-percentile values for a variety of anthropometric parameters, such as height, weight, organ mass, and total body mass, and are designed to represent average individuals in a patient population. They may be matched to individual patients by age. Reference phantoms are the basis for establishment of reference dose coefficients needed in prospective radiological protection programs, and for establishing means of verifying compliance with radiation protection standards. Nevertheless, they lack anatomical specificity for individuals who diverge from 50^{th} percentile parameters. By relaxing the restriction on 50^{th} percentile for the defining body morphometry parameters, one then defines a patient-dependent phantom, or more specifically, a phantom library, whereby the patient is matched to a given phantom in that library through not just age, but by both height and weight. Patient-dependent phantom libraries thus significantly improve the patient specificity of the dose estimate through closer matching of body shape. Depending upon the differential change in body shape – height, weight, body region circumference – a close or approximate match to a real patient may be made. The three morphometric category – patient-sculpted phantoms – take this a step closer by adjusting body surface control points of a patient-dependent phantom to unique and exactly match those of a given

patient. The major disadvantage of this approach is that the phantom is made uniquely for the patient in question, and thus no prior organ dosimetry library could be created, as is possible for patient-dependent phantom libraries. Patient-specific phantoms provide the most accurate match of both external as well as internal organ anatomy. They are created by segmenting whole-body CT scans to uniquely model a patient's exterior and internal organ morphometry. The requisite segmenting of the patient's CT images is a labor-intensive process and whole-body scans are often not available for patients. Consequently, patient-specific phantoms are often not used or created for organ dosimetry studies.

When using computational phantoms for medical dosimetry, the need for accuracy must be balanced with practicality. Patient-dependent phantoms provide an acceptable level of accuracy by modifying reference phantoms to match anthropometric parameters of patients, but remaining broad enough to represent a diverse population. Because patient-dependent phantoms must be created by modifying reference phantoms, it is necessary to work with hybrid phantoms due to their ability to be extensively deformed. Utilizing hybrid patient-dependent phantoms, phantom libraries can be created by matching statistically-analyzed anthropometric parameters to represent a population of individuals of varying body sizes and shapes. Phantom libraries are useful in radiation protection studies, as well as pre-computed dose libraries, and can be used to analyze changes in dose with varying body types.

Broggio *et a*l constructed a phantom library consisting of 25 whole body adult NURBS-based Caucasian phantoms with 109 identified organs or tissues.[3] Using a sampling strategy, 25 individuals were selected from the European Edition of the

Civilian American and European Surface Anthropometry Resource (CAESAR) database. The CAESAR database provides a mesh geometry of the outer body contour for individual volunteers subjected to exterior optical scanning. These body contours were then subsequently converted to NURBS surfaces for inclusion in the CAESAR library. Internal organs for the models were taken from the commercially-available organ sets provided by 3DSpecial (http://www.3dspecial.com/) and were resized using scaling factors incorporated into each model.[3] The body contour and internal organs and skeletal models were subsequently voxelized and merged together to create the final whole body adult phantoms.

In a study by Na *et al*, percentile-specific phantoms were created using computer algorithms to deform previously constructed base phantoms (RPI-adult male and RPI-adult female).[4] The internal organs within the phantoms were created using a commercial organ mesh dataset, AnatomiumTM 3D (http://www.anatomium.com/), and were scaled using computer algorithms to match volume and mass percentiles derived from International Commission on Radiological Protection (ICRP) Publications 23 and 89. To create varying whole-body sizes, anthropometric data (height and weight percentiles) for 19-year-old males and females were derived from the National Health and Nutrition Examination Survey (NHANES) database (1999-2002) and these parameters were matched by deforming another commercially available skin surface, MakeHuman™ (http://www.makehuman.org/).

Cassola *et al* created a library of 18 anthropometric phantoms (9 adult male phantoms and 9 adult female phantoms) based on 10th, 50th, and 90th mass and height percentiles of Caucasian individuals, extracted from the commercially available

ergonomic software PeopleSize.[5] The 3D modeling software Blender was used to deform previously constructed base phantoms, MASH3_sta (male adult mesh – standing) and FASH3_sta (female adult mesh – standing), to match the extracted height and weight parameters.[6] To resize internal anatomy, scaling factors were derived as a function of height based on an autopsy study done by de la Grandmaison *et al*.[7]

While the previously discussed studies represent comprehensive libraries of phantoms, the accuracy of commercially available outer body contours and internal organs is questionable. The outer body contours of Caucasian adult males taken from the CAESAR database are comprised of 412 individuals scanned in Italy and 566 individuals scanned in the Netherlands. Due to differing anthropometric features of individuals of different nationalities, the individuals found in the CAESAR database are not representative of the general Caucasian population, but rather a smaller subset. Like the CAESAR database, 3DSpecial offers a commercially available set of internal organs with little documentation in the study of their origin, thus the degree of their realism was not discussed in great detail.

Researchers at the University of Florida (UF) developed a family of hybrid phantoms constructed from NURBS surfaces, that contains a reference newborn, 1-year-old, 5-year-old, 10-year-old,15-year-old male and female, and adult male and female. The phantoms were developed to reflect the reference specifications found in ICRP Publication 89.[8] While maintaining anatomical realism, hybrid phantoms are also capable of having their internal and superficial anatomies altered due to the flexibility of the surfaces. In a study performed by Johnson *et al*, a methodology for constructing patient-dependent phantoms based on anthropometric percentile distributions from the

NHANES III database was derived to represent a distribution of the United States pediatric and adult populations.[9] The patient-dependent phantoms were then created by modifying a reference or "anchor" phantom from the UF family of hybrid phantoms to match predefined anthropometric parameters. In total, Johnson *et al* created 25 adult male and 15 pediatric female patient-dependent phantoms. The NHANES III database included anthropometric data for pediatric and adults collected from examinations from 1988-1994. To provide a more comprehensive library extension to represent the pediatric population and the rise in childhood obesity in the United States, this study was performed to provide a vital update and extension to the work done by Johnson *et al*.

In 2010, the Centers for Disease Control and Prevention (CDC) has estimated that roughly 12.5 million (17%) children and adolescents (ages 2-19) are obese in the United States, almost tripling the childhood obesity rate since 1980.[10] With these large increases, it is necessary to update the data from Johnson *et al* to reflect these changes. It is also necessary to abandon the previous method of age-based percentile anthropometric parameter calculations. Instead, grids based on height and weight bins that will capture all individuals and allow for varying growth rates of pediatric populations were created.

The purpose of this study was to create comprehensive grids for male and female pediatrics using more recent data from the NHANES database (1999-2006) to reflect obesity trends in the United States among this population. These grids will be used in the future to create a library of patient-dependent phantoms that represent pediatric populations. By selecting a weight column and height row from the pediatric

female grid, phantoms were constructed to investigate the role of height and weight variation on organ dose sensitivity for CT exams.

CHAPTER 2
MATERIALS AND METHODS

Statistical Analysis of National Health and Nutrition Examination Survey Data

Anthropometric pediatric data was obtained from the NHANES database conducted between 1999 and 2006 (which will further be referred to as the NHANES IV database for comparisons). Height and weight were chosen as primary parameters in the construction of a grid for pediatric males and females aged 2 to 20 (with a total of 17,028 individuals). Waist circumference, thigh circumference and arm circumference were included as secondary parameters. This library will serve as an update to the work performed by Johnson et al, which included data on individuals from 1988 to 1994 (NHANES III). The motivation for this update is the dramatic rise in childhood and adult obesity over the intervening years in the United States. Due to the unavailability of average sitting height and buttocks circumference in the database applied in this study, these values were interpolated from the prior NHANES III database to match the heights and weights of the individuals in the updated grid.

Master's student Shannon O' Reilly at the University of Florida analyzed male and female pediatric individuals independently and binned by height increments of ±5 cm, ensuring that the 5th and 95th height percentiles were captured using a MATLAB Gaussian fitting program. Each height bin was further parsed by weight increments of ±2.5 kg, with each weight bin containing data for at least ten individuals to assure statistical significance. For each height-weight bin, secondary parameters including the average circumferences of the arm, waist, and thigh were determined, along with sitting height and buttocks circumference from the previous NHANES database. For a small number of weight extremes not all secondary parameters contained the necessary ten

individuals for a statistically significant result, so linear interpolation was used to determine the proper circumferences. Using primary and secondary parameters, a grid containing 85 male height-weight bins and a grid containing 73 female height-weight bins were constructed. These grids will provide the blueprints for later constructing a comprehensive library of patient-dependent phantoms containing 158 pediatric phantoms.

Reshaping of Reference Phantoms

Due to the recent obesity trends, it was necessary to update the UF/NCI family of reference hybrid phantoms to reflect these trends. To begin this update, the primary parameters of height and weight were left unchanged to match ICRP reference values, while the secondary circumference parameters were revised. This process included a double linear interpolation of the circumference data. The first interpolation of the circumference data was done to match the ICRP reference weight, while the second interpolation was to match the height. In cases that lacked sufficient circumferential data to allow for interpolation, extrapolation based on the least squares method was used to obtain the circumference. Updated circumferences were calculated for each phantom in the current UF/NCI reference phantom library, excluding the newborn and 1 year old since this data was not acquired from the NHANES database.

After calculating updated circumference data, the phantoms were then reconstructed by Dr. Choonsik Lee, investigator at the National Cancer Institute in the Division of Cancer Epidemiology and Genetics. Circumferences on the phantoms were matched within 3% of targeted values and the total body of the phantom was modified to compensate for circumference adjustments to match ICRP reference masses within 1%.

Body Mass Index Analysis

To further aid in the construction of the pediatric phantom library, body mass index (BMI) calculations were performed for each height-weight bin within the grids. Because the scaling of phantoms can become quite labor-intensive, requiring additional steps for overweight individuals (detailed in a later section), it can be useful to know the weight category (underweight, healthy, overweight, or obese) prior to the scaling process. An individual's BMI is a reliable indication of weight category and can be calculated for pediatrics with relative ease. To calculate the BMI for each pediatric height-weight combination within the grids, the individual's mass (in kilograms) is divided by their height (in meters) squared. For adults, this calculated number would then fall within an acceptable range for each weight category. For pediatric individuals, weight categories are not determined as easily due to body development during the pediatric years. To determine a weight category, an average age of the individual in each bin was estimated using the ages of the individuals that were refined by height (bin height – bin height + 0.9 cm) and weight (bin weight – bin weight ± 2.5 kg). Since BMI calculation was used only to predict a rough estimate of body size, it should be noted that average age calculations did not require the minimum of 10 individuals per calculation. After obtaining a BMI calculation and average age for each height-weight combination on the grids, BMI-for-age charts provided by the CDC were used to determine a BMI percentile for each individual. BMI percentile ranges then were used to determine the weight category of each individual. BMI percentiles below the 5^{th} percentile are considered underweight individuals, while percentiles ranging between 5^{th} percentile and less than 85^{th} percentile represent healthy individuals. Percentiles ranging between 85^{th} percentile and below 95^{th} percentile are considered overweight.

Percentiles equal to or greater than the 95th percentile are considered obese. The pediatric grids were then color-coded based on these weight categories.

Patient-Dependent Phantom Construction

In this study, 20 patient-dependent phantoms were constructed to aid in CT dosimetry and dose sensitivity analysis. To aid in the construction of the phantoms, both grids were redesigned to detail whichever reference phantom would serve as the anchor phantom in the scaling process, and determine whether the height would be scaled up or down. Since the effects of height and weight on dose were of interest in this study, five female pediatric phantoms with a total body mass of 50 kg were made, at 135 cm, 145 cm, 155 cm, 165 cm, and 175 cm standing heights. Additionally, 16 female pediatric phantoms were constructed at a fixed height of 165 cm with weights ranging between 40 kg and 115 kg, at 5 kg increments (one phantom was previously constructed at this height when the fixed-weight phantoms were created and did not need to be made again). Along with matching the heights and weight detailed within the grid, secondary circumference parameters at each grid point were also matched.

The scaling process is this study mimics methods previously used by Johnson *et al* and begins with selecting an appropriate anchor phantom from the phantom-mapped grid importing it into the NURBS modeling software Rhinoceros 4.0.[9] Initially, the sitting height of the anchor phantom was measured as the distance between the top of the head to the bottom of the ischium. The ratio of the targeted sitting height defined in the grid to the measured sitting height produced a scaling factor. The head, torso, and arms (including all internal organs and bony anatomy) were scaled uniformly in 3-D by this scaling factor, with the bottom of the ischium acting as the scaling point of origin. To match the target standing height of the phantom, the legs were scaled in the z-direction

by a scaling factor equal to the ratio of measured leg length to targeted leg length (coordinate system shown in Figure 2-1). With the proper standing and sitting heights matched, the secondary circumferential parameters were then matched. To assure consistency between anchor phantoms for circumferential measurements, a separate layer was added to each anchor phantom with reference planes placed as markers for circumference measurements. These planes were placed at the points of measurement of the circumferences as defined by the CDC. Control points on the outer body contour were modified to simulate a change in adipose tissue thickness to match circumferences. For phantoms with waist circumferences smaller than the waist circumference of the anchor phantom, a 2D scale was applied to the phantom in the x-y plane to accommodate changes to circumferences while preserving previously matched height requirements. For obese phantoms, arms and legs were rotated outward to avoid an overlap of outer body contours due to the increased circumference values. Once circumferences were matched, control points near to the point of circumference measurements were visually analyzed and fine-tuned to preserve correct body shape.

To complete the phantom scaling process, total body mass was iteratively matched by adjusting the control points of the outer body contour (adipose tissue) in areas that were not restricted by secondary parameters. These areas of the body include lower arms and legs, upper torso, and adipose tissue of the breasts. Total body mass was estimated in Rhinoceros^{TM} using the volume calculation tool and tissue densities. Five distinct tissue types were defined as adipose tissue, cartilage, homogenous bone, lung, and residual soft tissue and used to calculate the total body mass. Volumes of cartilage, bone (cortical), lungs, muscle, and outer body contour were

calculated initially. When calculating the volume the outer body contour body, all objects within this layer were first joined using the Boolean Union tool in Rhinoceros to eliminate any overlap between surfaces. The volume of adipose tissue was estimated by subtracting the volume of the muscle layer from the outer body contour volume. The volume of the bulk soft tissue was found by subtracting the volumes of the bone, cartilage, and lungs from the muscle volume. Total body mass was found by multiplying the volumes of adipose tissue, bone, lungs, cartilage, and residual soft tissue by their respective densities and summing these masses.

Computed Tomography Simulated Exams

In collaboration with Mr. Daniel Long, PhD student in medical physics, the effect of body morphometry on organ doses for a chest-abdomen-pelvis (ranging from the thoracic inlet to the lesser trochanters) CT scan was assessed by simulating a Siemens Sensation 16 CT scanner using the Monte Carlo transport code MCNPX2.6 (using 100 million particle histories) and performing on 20 phantoms. To adequately compile a comprehensive database of varying body morphometries, 5 phantoms were constructed at height increments of 10 cm, starting with 135 cm at a fixed weight of 50 kg to assess the effects of height on organ doses. The effects of weight on organ doses were assessed using 16 phantoms constructed at weight increments of 5 kg, starting with 40 kg, at a fixed height of 165 cm. Phantoms using adult and 15-year-old anchor phantoms were voxelized to resolutions of 3 x 3 x 3 mm^3 and phantoms using the 10-year-old anchor phantom were voxelized to a resolution of 2 x 2 x 2 mm^3. The scan parameters for each simulation were beam energy of 120 kVp, body filter, pitch of 1.0 (1.375 for the phantoms at a fixed weight), effective mAs of 100, and a 2.4 cm beam collimation. The

scan ranged from the thoracic inlet to the lesser trochanter on each phantom. Additional information on the CT simulation can be found in Appendix A.

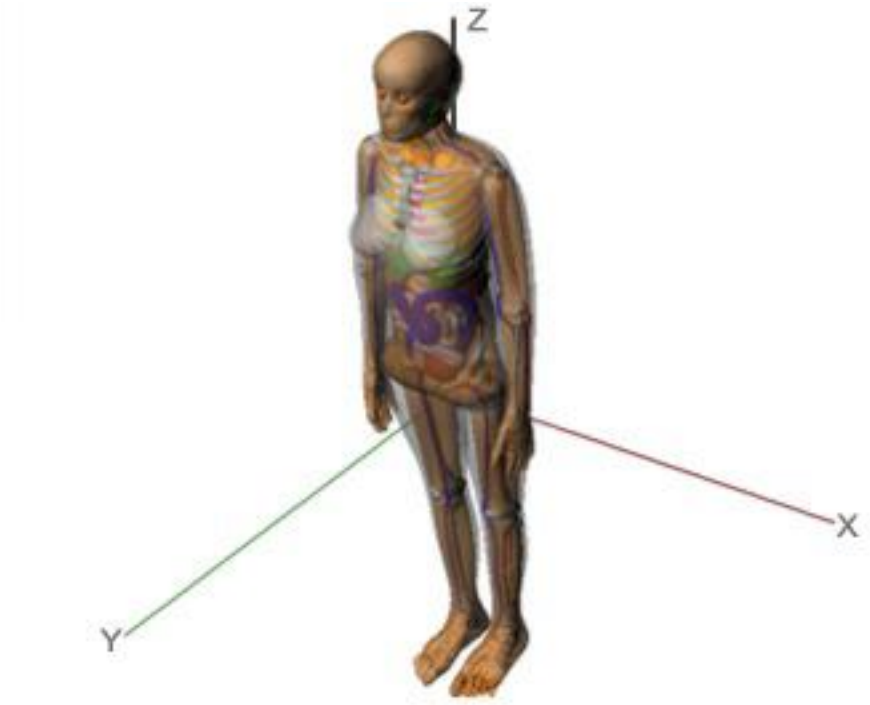

Figure 2-1. Perspective view of adult female reference phantom demonstrating the coordinate system used during the phantom scaling process.

CHAPTER 3
RESULTS AND DISCUSSION

Obesity Trends

Figures 3-1 and 3-2 show the percentage of obese pediatric individuals as a function of standing height for both NHANES databases. The percentage of obese individuals increases with standing height for both male and female pediatric populations. Consistent with the previously mentioned CDC estimates for obesity, the percentage of obese individuals is higher in the more recent NHANES IV database when compared with the NHANES III database. This is true in all cases except males and females with standing heights of 85 cm, and females with a standing height of 125 cm. Tables 3-1 and 3-2 quantify the percent difference between pediatric individuals in either NHANES database, showing an average increase of 33.71% in the percent of obese individuals for males, and 23.01% for females.

Updated Reference Phantoms

Using the data collected in the NHANES IV database, reference phantoms were updated to match secondary circumference data interpolated from the database based on ICRP 89 reference heights and weights. Updates to circumferential data also corrected for an anatomical discrepancy in the phantom outer body shape. Previously, the buttocks circumference in all phantoms, excluding the 15-year-old and adult female phantoms, was found to be less than the waist circumference. This trend was not consistent with circumference values seen in the database, which showed a buttocks circumference larger than waist circumference. Table 3-3 shows the measured, suggested updates, and revised circumferential data for all reference phantoms that were updated. For consistency, all circumference measurements were made using

previously discussed measurement planes. The revised circumferences were matched to the suggested updated dated values within 3%. Once circumferences were matched within 3%, organ masses, total body mass and separable fat mass were matched within 3% of ICRP 89 reference values. The updated reference phantoms are shown in Figure 3-3.

Phantom Library Grids

The final height/weight grid for pediatric males and females are show in Figures 3-4 and 3-5, respectively. The grids are color-coded to indicate the phantom classification as underweight, healthy, overweight, or obese based on BMI percentile analysis CDC definitions of body morphometry. In total, the grids target 85 pediatric males and 73 pediatric females. When viewing the grids in Microsoft® Excel, secondary circumferential data is displayed in a comment box that opens when selecting a cell of interest, demonstrated in Figure 3-6. Target secondary circumferential data, as well as average sitting height, for male and female pediatric phantoms are shown in Tables 3-4 and 3-5, respectively. To aid in the phantom construction process, a second set of grids were created to incorporate the 3-D up- or downscaling- methodology of the reference phantoms. These grids are shown in Figures 3-7 and 3-8 for male and female pediatrics, respectively. The color-coding of these grids indicates the reference phantom that will be used initially in the scaling process. The direction of the arrow found in each cell indicates either a three-dimensional up- or down-scaling to the reference phantom torso, arms, and head to match targeted sitting height values.

Patient-Dependent Phantom Library Subset for Computed Tomography Dosimetry

A subset of patient-dependent phantoms was created from the pediatric female grid to explore the effects of height and weight on organ doses in a simulated CT examination. To investigate the effect of weight on organ doses, 16 patient-dependent phantoms were created at a fixed standing height of 165 cm. The weights for these phantoms ranged between 40 kg and 115 kg in 5-kg increments. A selection of these phantoms is displayed in Figure 3-9. Additionally, to analyze the effects of patient height on organ dosimetry, 5 patient-dependent phantoms were created at a fixed weight of 50 kg, weight heights ranging from 135 cm to 175 cm, in 10 cm increments. These phantoms are displayed in Figure 3-10. When constructing the 20 patient-dependent phantoms, total body mass was matched to targeted values within 1 kg, and all height and secondary circumferential data were matched to targeted values within 1%. After their construction, all phantoms were voxelized using the MATLAB^{TM} code Voxelizer v9.2. Post-voxelization total body masses matched the pre-voxelization masses within 1% and targeted total body mass values within 1 kg.

Computed Tomography Organ Dosimetry

To assess the effect of standing height on organ dosimetry, five patient-dependent phantoms were created and 120 kVp CT simulations were performed using MXNCPX2.6 for each phantom with a pitch of 1.375. A summary of these organ doses can be found in Table 3-6. To better correlate the effects of height on organ dose, organ doses for organs in the beam were plotted as a function of height in Figure 3-11. As height increases, internal organs are scaled with the head and torso region to match targeted sitting height values. Due to this scaling, organ volumes are increasing with

height. Similarly, for phantoms in which the reference waist circumference was significantly larger than targeted circumferential values, the torso/head regions were scaled in two-dimensions to accommodate a smaller waist circumference (165 cm and 175 cm phantoms). This also changes organ volumes. These changes to organ volume result in significant organ variation, making dose correlations very difficult. Figure 3-11 depicts this organ dose variability, most significantly in the kidneys and spleen.

Adjusting the scan to a pitch of 1, Monte Carlo CT simulations were performed on 16 patient-dependent phantoms to investigate the effect of weight on organ doses. The arms were removed (excluding the femoral head) from each phantom to mimic clinical conditions in which the patients would be positioned with their arms raised above their head for the examination. Organ doses for these simulations can be found in Table 3-7. For organs in the beam, organ doses as a function of weight are plotted in Figure 3-12. Figure 3-12 shows the predicted downward trend of in-field organ doses, with a fixed effective mAs of 100, with increased patient weight due to increased adipose tissue. Slight “rippling” in data is seen that could be attributed to statistical variation. These slight dips and rises in the data as weight increases could also be due to varying distributions of adipose tissue in each phantom due to the phantom-scaling process. For example, Figure 3-12 depicts a sharp increase in the lung dose of the 100 kg phantom, relative to the 95 kg phantom. Upon inspection of the phantoms, the volume of breast tissues in the 95 kg phantoms is significantly larger than that of the 100 kg phantoms, which could contribute to a decrease in lung dose. Similar adipose tissue redistributions for higher-mass phantoms could account for discrepancies in organ doses.

Organ Dose Interpolation

Upon completion of the pediatric male and female patient-dependent libraries, UF will be working with NCI to construct a CT dose library to later be used for patient-dose tracking. Though all 158 pediatric phantoms will be available in their original NURBS/polygon mesh format, the possibility exists to create a coarse sampling of this library to be voxelized and imported into MCPNX for organ dose library generation. Using this smaller voxelized phantom library, the extent to which organ doses can be interpolated for phantoms that were not voxelized was investigated. Because organ doses followed predicted trends for the 16 phantoms created at a fixed-height of 165 cm, interpolation was performed using this subset of the patient-dependent phantoms created for CT dosimetry.

To begin this investigation, the 16 patient-dependent library of calculated CT organ doses was further parsed to include only 8 phantoms, removing every other phantom (10 kg intervals). Using the organ doses for in-field organs, data points were fit with a second-degree polynomial trendline using Microsoft® Excel (with R^2 values greater than 0.95). Using the equation of each unique trendline for its respective organ, organ doses were calculated for the phantoms that were previously removed from the library. The percent difference between interpolated and Monte Carlo calculated organ doses can be found in Table 3-8. This same method was used when interpolating between phantoms at 15 kg intervals, 20 kg intervals, and 25 kg intervals and percent difference can be found in Tables 3-9, 3-10, and 3-11, respectively. Generally, organ dose interpolation with each level of coarseness proves efficient and beneficial, with low percent errors. For heavier phantoms (larger than 70 kg), percent differences increase due largely to the previously discussed “rippling” effect depicted in Figure 3-12.

When interpolating organ doses after removing every other phantom, 22.79% of interpolated doses had percent differences between 5% and 10% of original organ doses values. Interpolated organ values with percent differences greater than 10% were present for phantoms with total body masses 85 kg and greater, accounting for 13.97% of the total interpolated values. After interpolating between phantoms at 10 kg intervals, organ dose values with percent differences between 5% and 10% accounted for 21.18% of total interpolated organ dose values. Only 5.29% of all interpolated values had percent differences greater than 10% and were found only in phantoms with total body mass equal to or greater than 90 kg. Interpolated organ doses with percent differences 5% to 10% from original organ doses values accounted for 18.62% of all interpolated values for phantoms at 15 kg intervals. Percent differences greater than 10% accounted for only 16.17% of all interpolated values and were present in phantoms with total body masses greater than or equal to 85 kg. Lastly, when interpolating between phantoms at 20 kg intervals, percent differences ranging between 5% and 10% accounted for 20.58% of all interpolated values. Percent differences greater than 10% for interpolated organ doses accounted for 12.75% of all interpolated values and were seen in lighter individuals, as well as individuals with larger total body masses.

From these calculations, removing every two phantoms proves to be the more efficient and accurate method of interpolation for phantoms at a fixed height with varying weights. This method is most effective for phantoms with total body masses less than 90 kg, with interpolated organ dose percent differences less than 10% from original values.

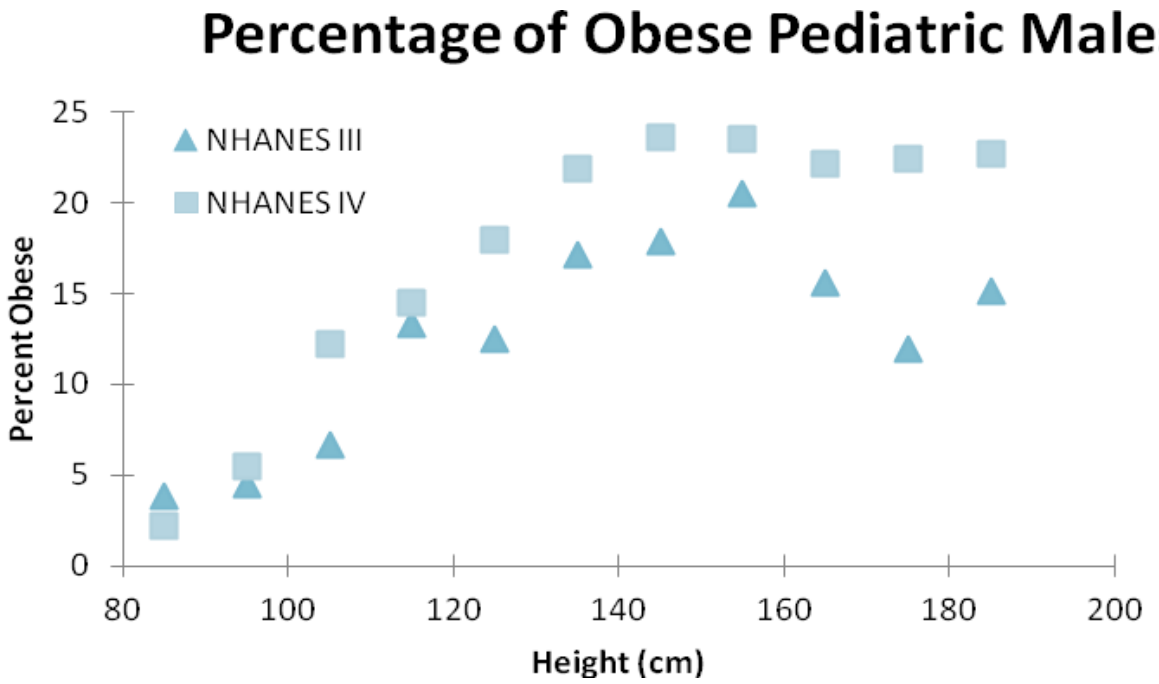

Figure 3-1. Percent of pediatric male individuals that are obese as a function of standing height.

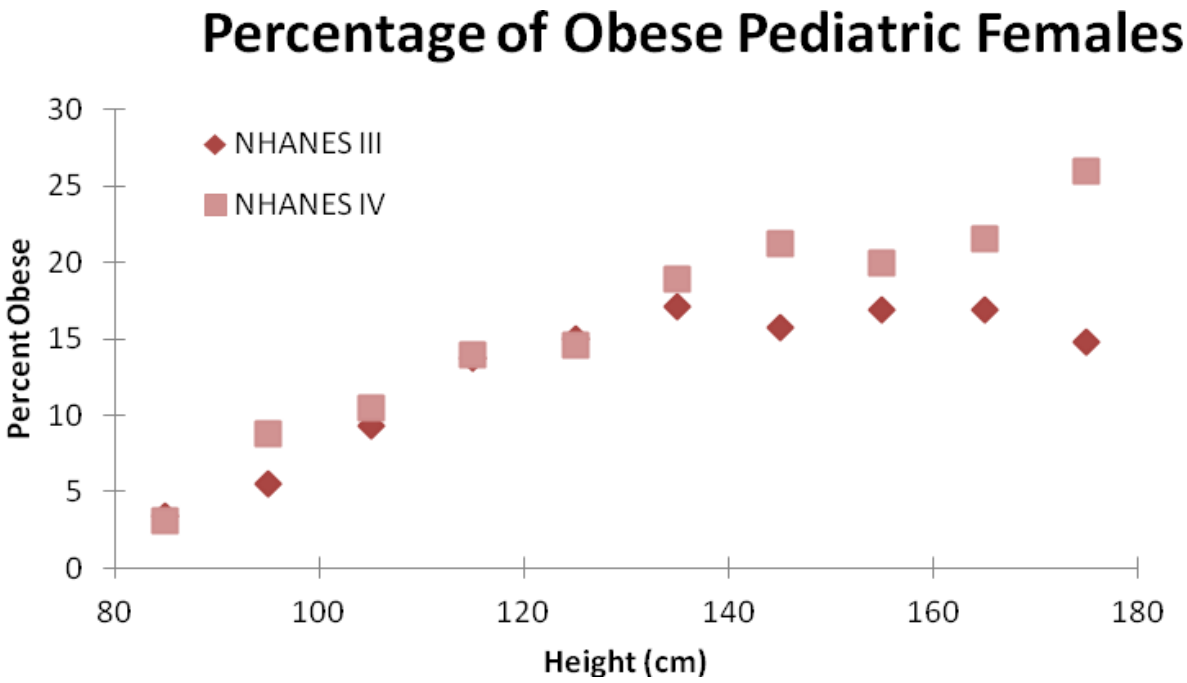

Figure 3-2. Percent of pediatric female individuals that are obese as a function of standing height.

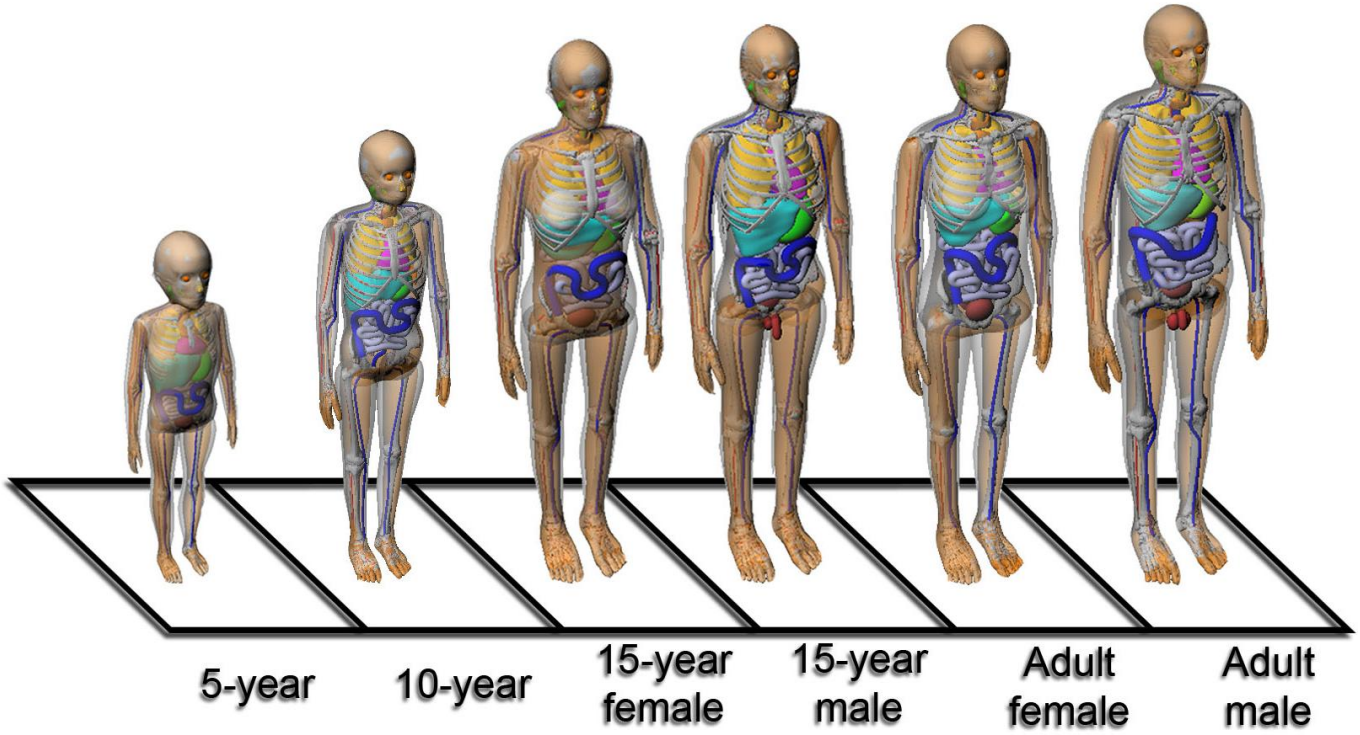

Figure 3-3. UF/NCI series of ICRP89 compliant hybrid reference phantoms

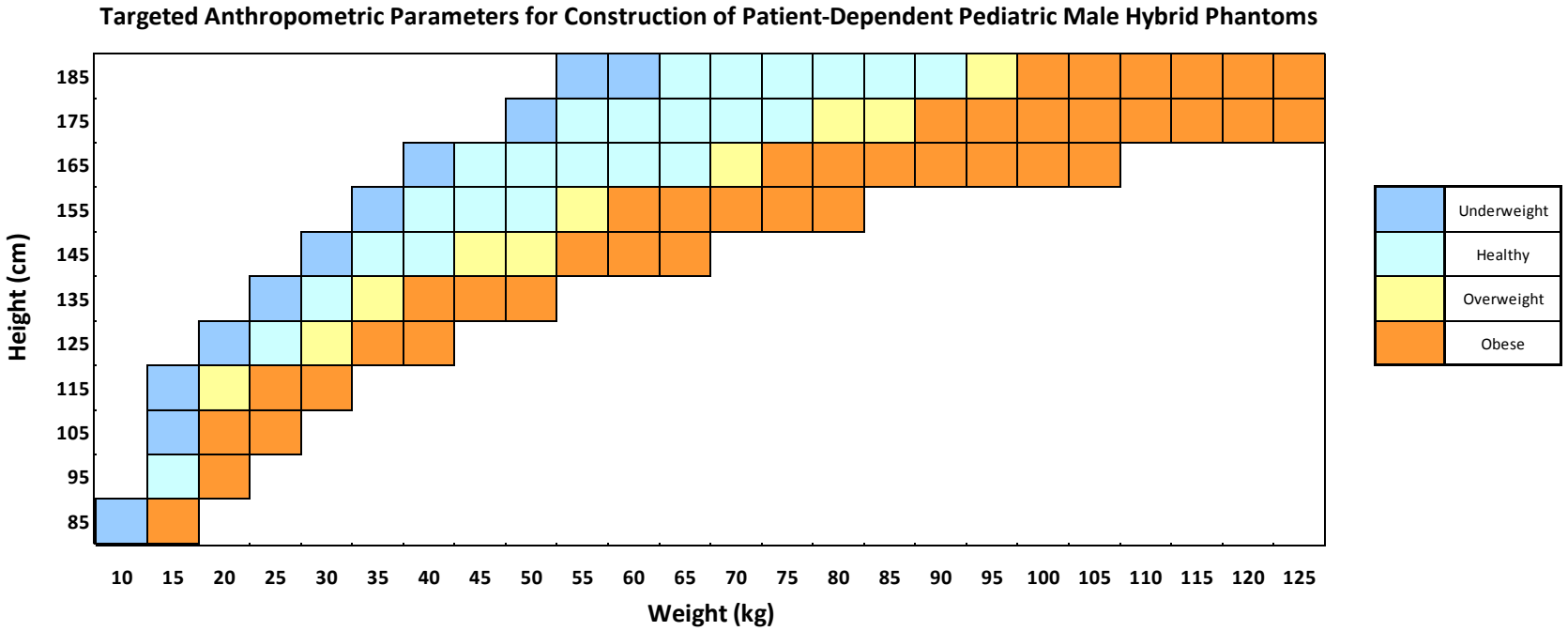

Figure 3-4. Targeted grid for the UF/NCI library of pediatric male hybrid phantoms. Color code indicates the phantom classification as underweight, healthy, overweight, or obese based upon BMI percentiles and CDC definitions of body morphometry.

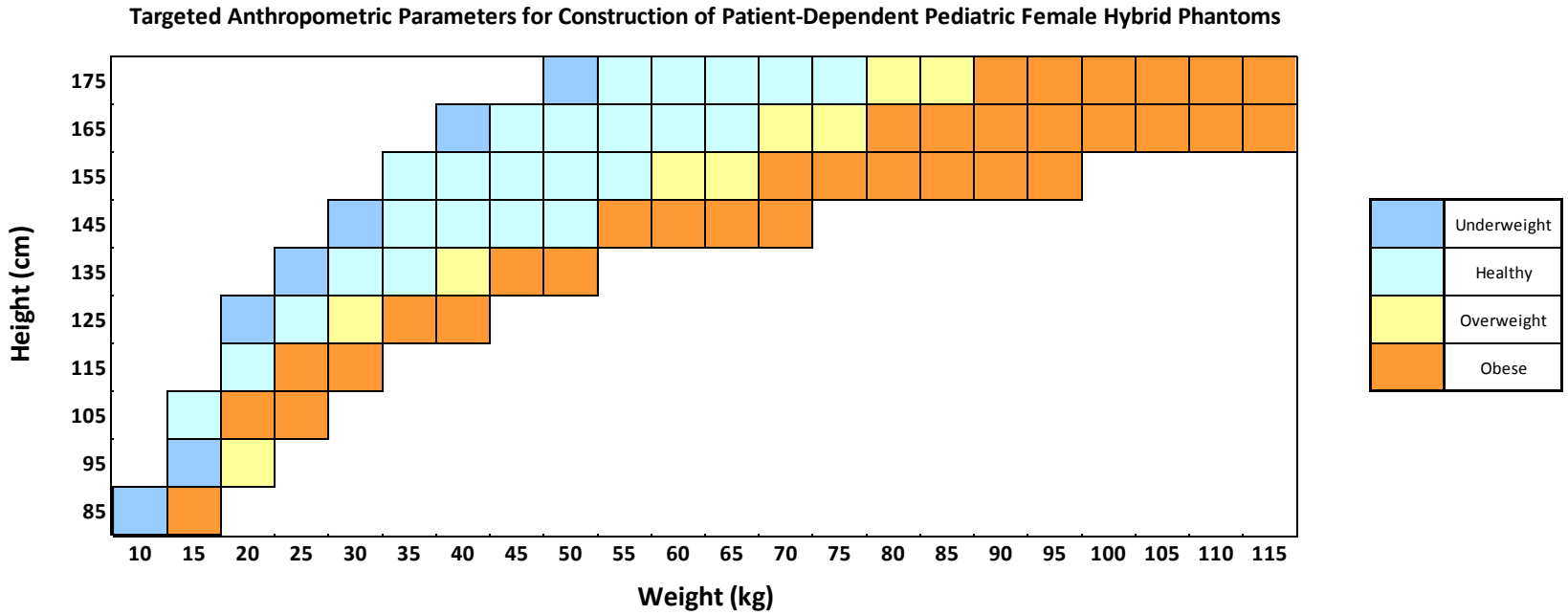

Figure 3-5. Targeted grid for the UF/NCI library of pediatric female hybrid phantoms. Color code indicates the phantom classification as underweight, healthy, overweight, or obese based upon BMI percentiles and CDC definitions of body morphometry.

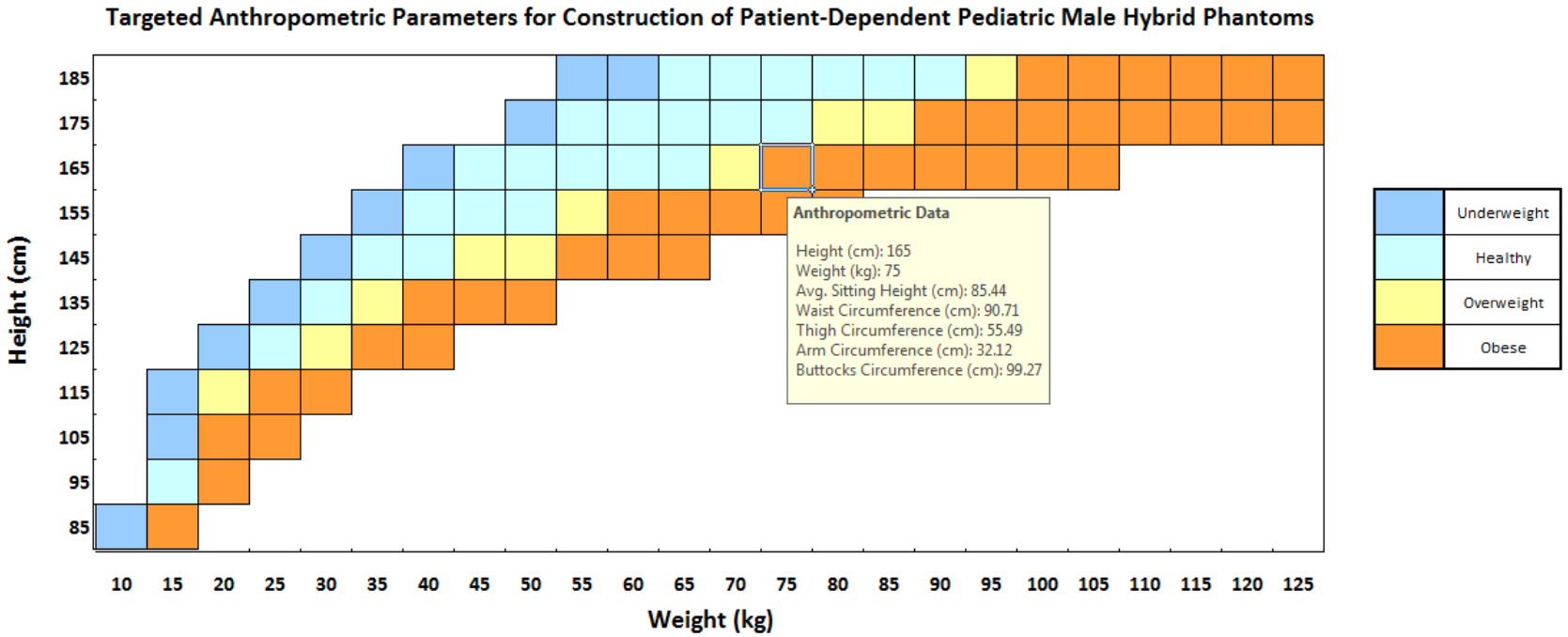

Figure 3-6. Targeted grid for the UF/NCI library of pediatric male hybrid phantoms. Comment box opens upon selection of desired cell to display height, weight, average sitting height, and secondary circumferential data.

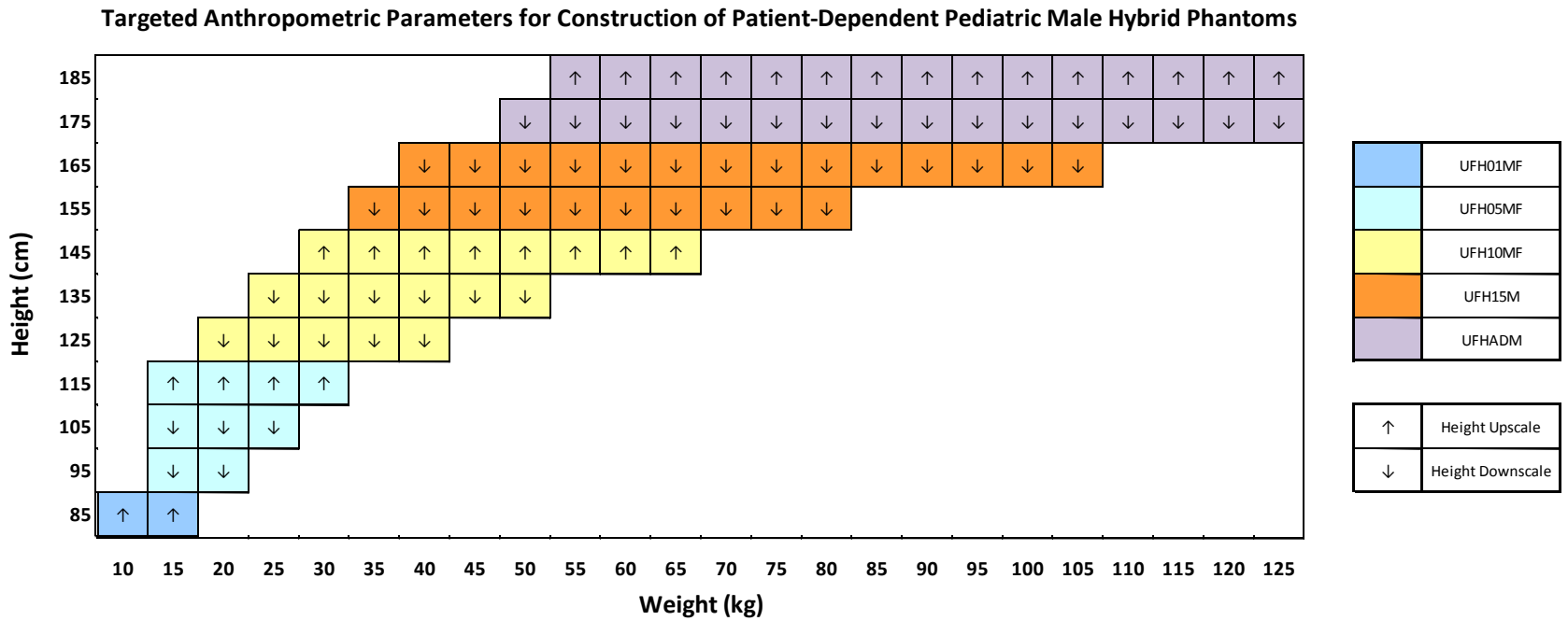

Figure 3-7. Construction methodology for UF/NCI library of pediatric male hybrid phantoms based upon 3D proportional scaling of existing UF/NCI reference phantoms to match targeted values of sitting height.

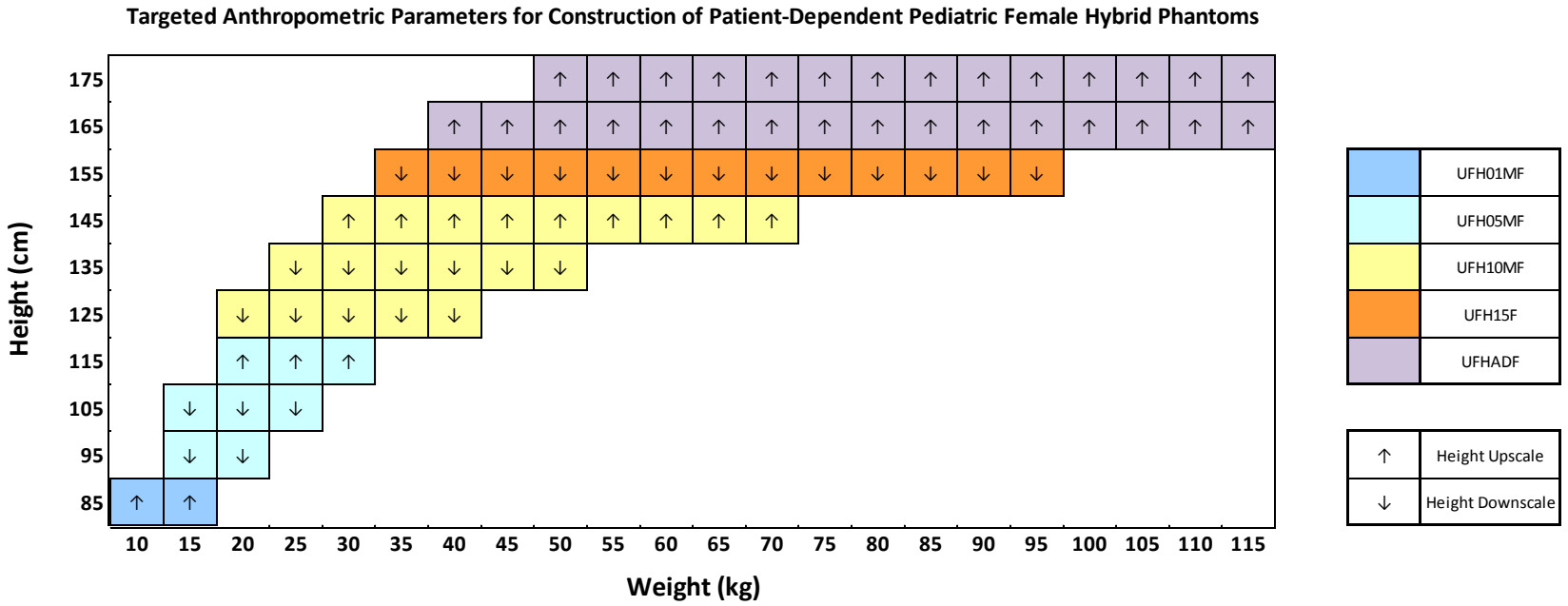

Figure 3-8. Construction methodology for UF/NCI library of pediatric female hybrid phantoms based upon 3D proportional scaling of existing UF/NCI reference phantoms to match targeted values of sitting height.

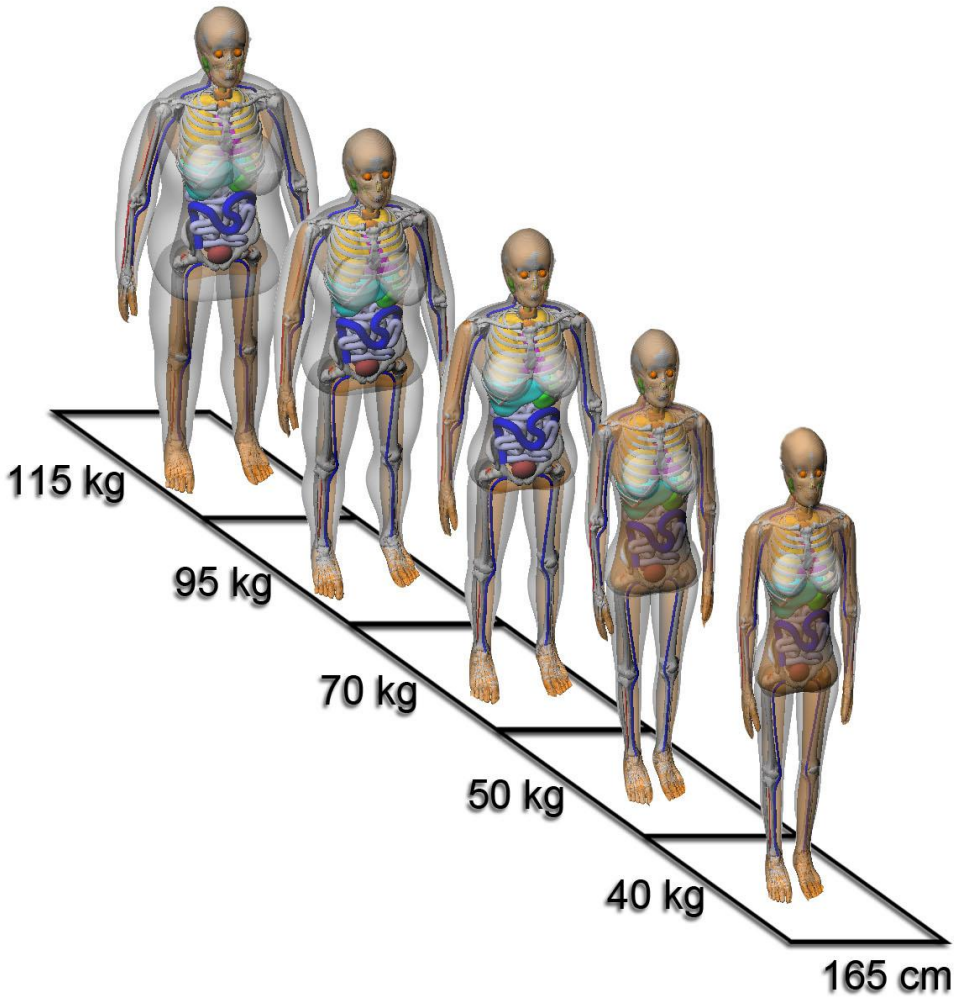

Figure 3-9. Selection of phantoms at a fixed height of 165 cm at varying weights.

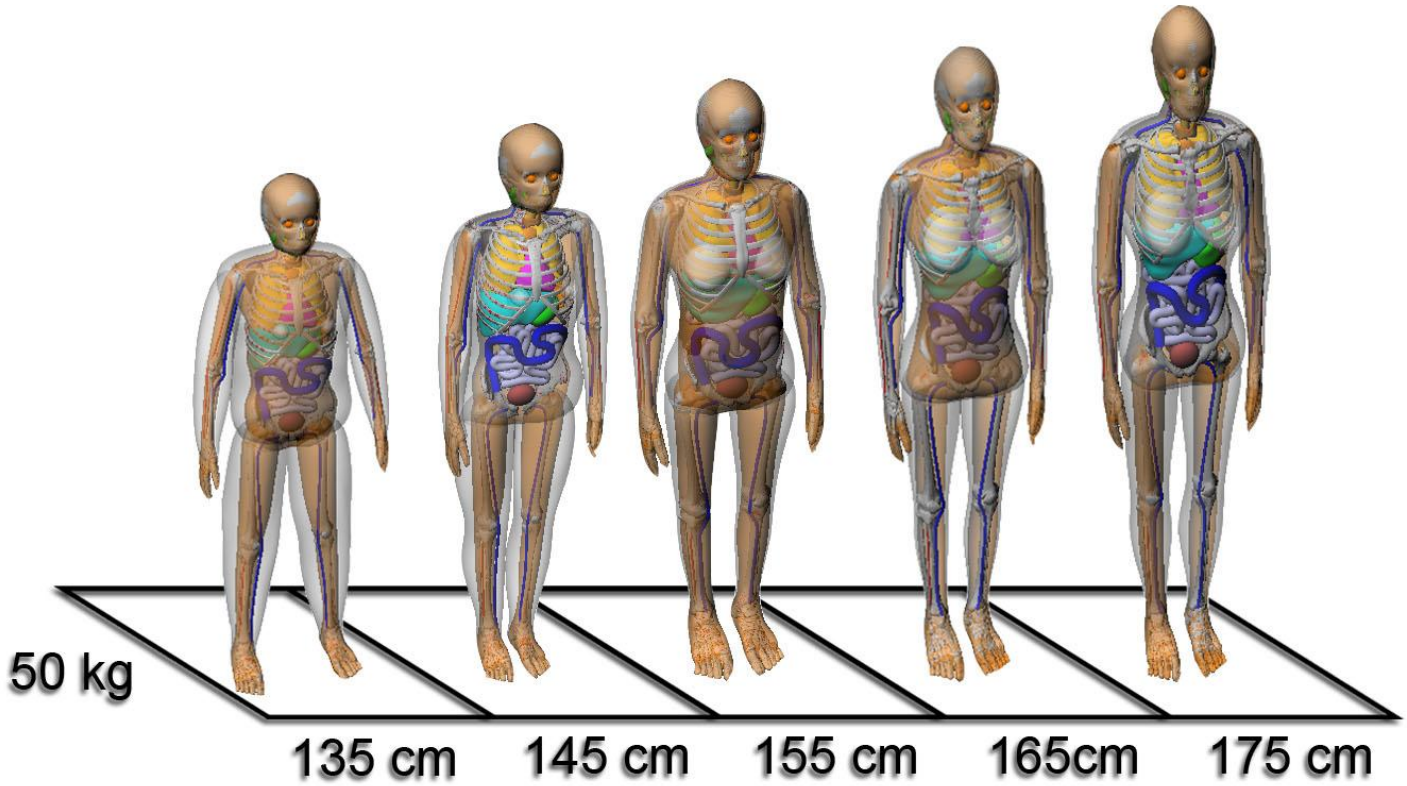

Figure 3-10. Phantoms at a fixed weight of 50 kg at varying heights.

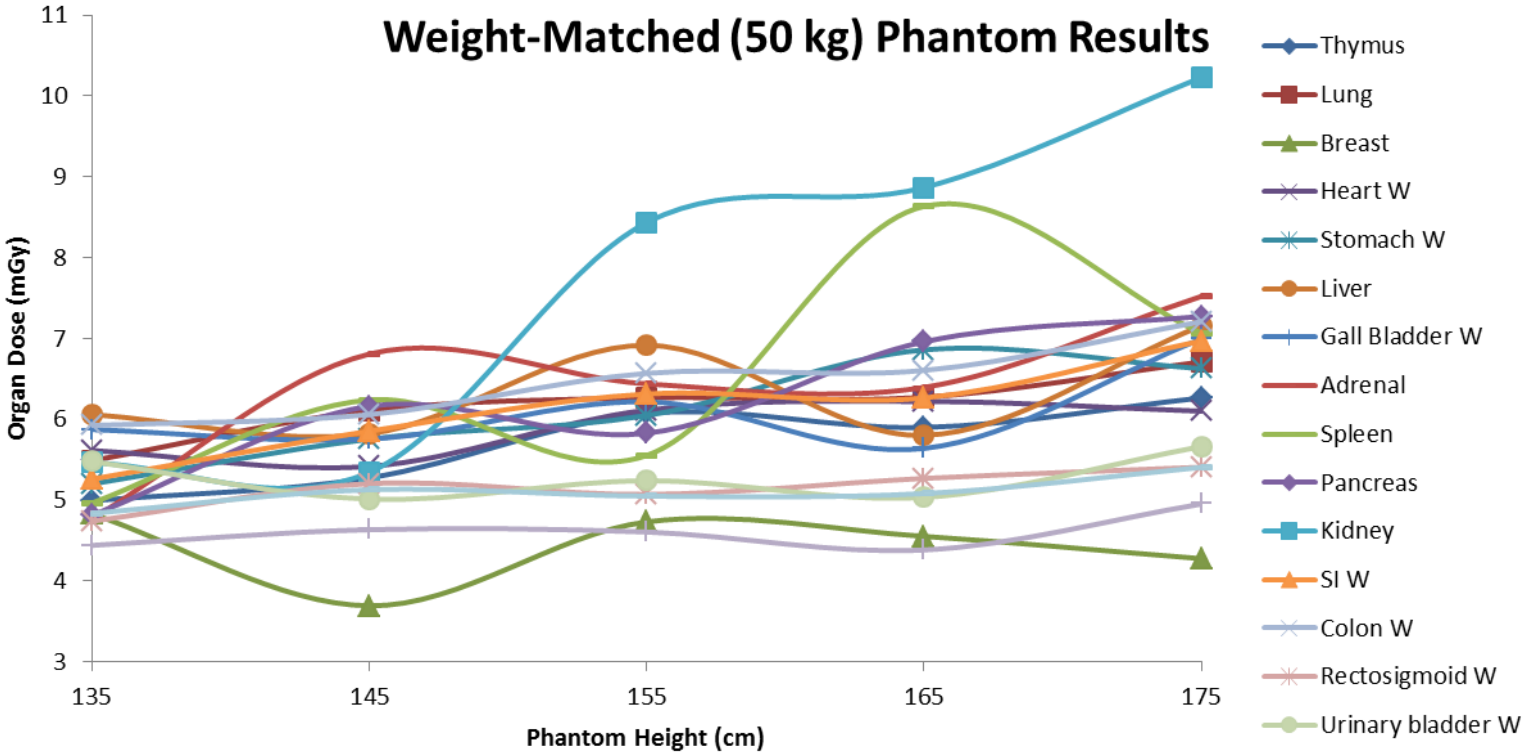

Figure 3-11. Organ doses as a function of height for organs in the beam for a CAP CT scan at 120 kVp, with effective mAs of 100 and pitch of 1.375.

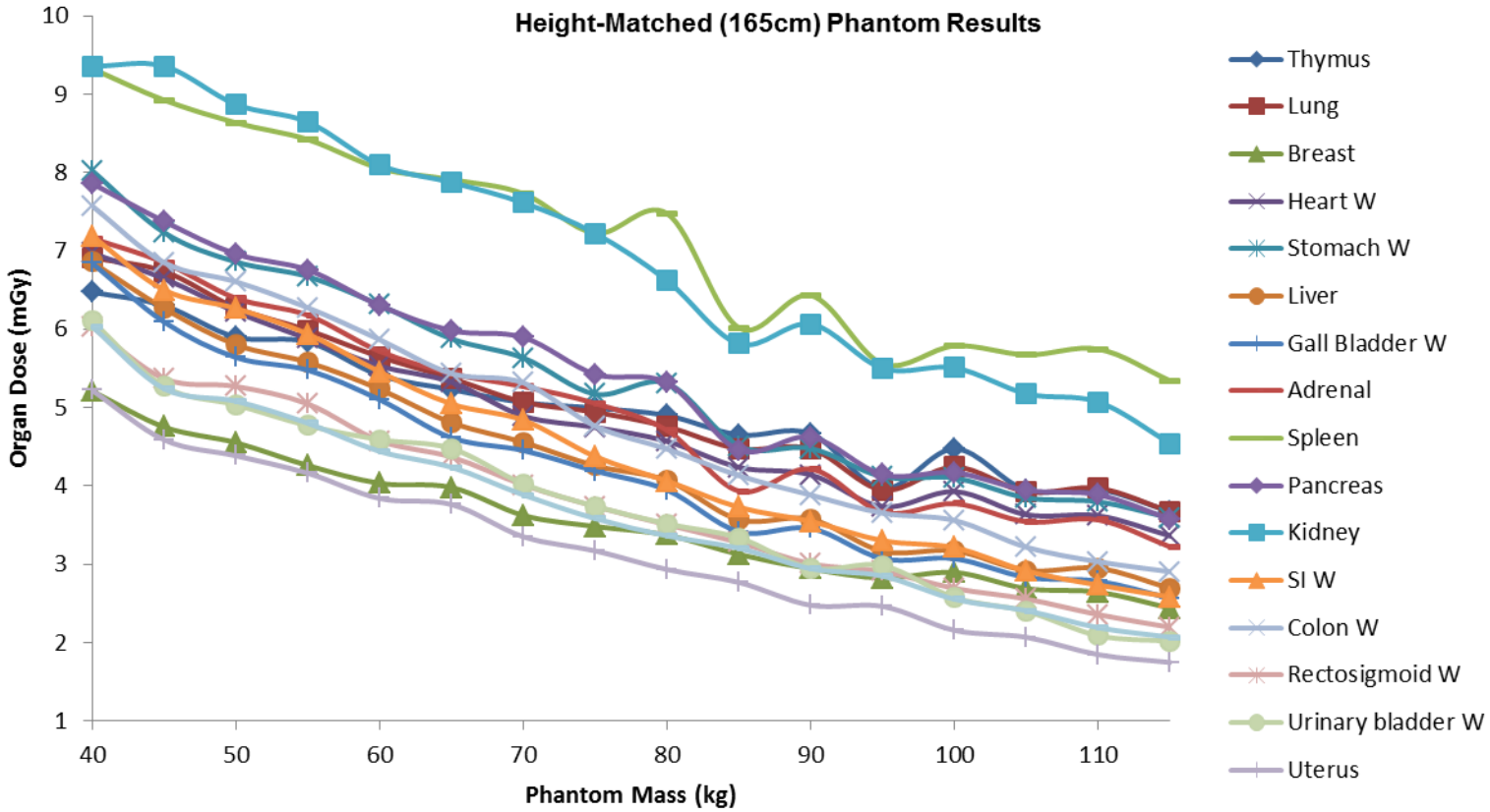

Figure 3-12. Organ doses as a function of weight for organs in the beam for a CAP CT scan at 120kVp, with effective mAs of 100 and pitch of 1.0.

Table 3-1. Percent difference summary for pediatric males between NHANES databases.

Height	NHANES III	NHANES IV		% Difference
85	3.79	2.21		-41.66
95	4.49	5.49		22.17
105	6.67	12.26		83.85
115	13.32	14.51		8.92
125	12.45	17.92		44.01
135	17.18	21.83		27.11
145	17.90	23.57		31.65
155	20.52	23.52		14.63
165	15.54	22.13		42.40
175	11.96	22.42		87.44
185	15.10	22.70		50.30
			Average	33.71

Table 3-2. Percent difference summary for pediatric females between NHANES databases.

Height	NHANES III	NHANES IV		% Difference
85	3.36	3.11		-7.46
95	5.56	8.83		58.92
105	9.36	10.49		12.07
115	13.71	13.93		1.58
125	14.97	14.60		-2.45
135	17.08	18.86		10.40
145	15.78	21.22		34.50
155	16.86	19.92		18.15
165	16.86	21.58		28.01
175	14.74	26.01		76.42
			Average	23.01

Table 3-3. Updated circumference values for reference phantoms.

	Circumference (cm)															
	Waist				Buttocks				Arm				Thigh			
Phantom	Meas.	Updated Target	Revised Reference	Diff (%)	Meas.	Updated Target	Revised Reference	Diff (%)	Meas.	Updated Target	Revised Reference	Diff (%)	Meas.	Updated Target	Revised Reference	Diff (%)
UFH05MF	57.7	52.5	54.2	3%	58	56.2	57.7	3%	14.8	17.5	17.5	0%	26.4	31.2	30.9	-1%
UFH10MF	70.9	61.2	63.1	3%	72.5	70.4	70	-1%	21.4	20.7	21.4	3%	31.6	38.2	37.6	-2%
UFH15M	89.9	72.2	74.4	3%	85	86.1	86.5	0%	27.2	26.6	27.2	2%	35.6	47	45.8	-3%
UFH15F	76.9	73.4	75.9	3%	80.5	89.6	88.8	-1%	27.7	25.4	25.4	0%	43.5	46.7	46.4	-1%
UFHADM	97.9	89.3	92	3%	96.3	94.9	96.3	2%	27.3	30.8	31.1	1%	39.9	49.4	48.2	-2%
UFHADF	84.8	81.8	83.7	2%	93.8	95.9	93.8	-2%	29	27.8	28	1%	39.6	47.9	47.6	-1%

Table 3-4. Targeted heights, weight, and circumferential data for male pediatric phantoms.

Standing Height (cm)	Average Sitting Height (cm)	Weight (kg)	Waist Circumference (cm)	Average Buttocks Circumference (cm)	Thigh Circumference (cm)	Arm Circumference (cm)
85 cm	50.26	10	45.28	48.02	0.00	15.08
		15	48.47	50.93	0.00	16.36
95 cm	53.27	15	48.95	51.43	0.00	16.40
		20	56.46	57.12	0.00	18.91
105 cm	57.00	15	49.48	52.61	0.00	16.32
		20	53.58	56.22	0.00	18.03
		25	64.46	64.31	0.00	20.99
115 cm	61.08	15	48.32	52.33	0.00	15.88
		20	52.67	57.43	31.90	17.52
		25	58.22	62.73	35.43	19.60
		30	68.69	69.82	38.95	23.00
125 cm	65.47	20	52.06	58.43	30.95	17.06
		25	56.09	62.67	34.48	18.79
		30	62.70	68.75	38.14	21.22
		35	70.47	76.51	43.12	23.60
		40	78.95	81.02	46.19	26.45
135 cm	69.70	25	55.25	63.81	34.04	18.28
		30	59.04	67.85	37.12	20.03
		35	65.25	73.03	40.83	22.33
		40	72.95	78.57	43.96	24.33
		45	79.30	83.91	46.95	26.45
		50	87.02	88.68	49.50	27.91
145 cm	73.80	30	57.89	67.64	36.16	19.46
		35	61.63	72.10	39.33	21.18
		40	67.20	76.68	42.26	23.22
		45	73.66	81.98	45.76	25.18
		50	80.76	86.51	48.15	27.13
		55	85.18	89.88	50.78	28.80
		60	90.54	93.53	52.93	30.53
		65	96.78	96.97	55.12	31.61
155 cm	78.67	35	60.83	72.79	38.34	20.39
		40	63.99	75.01	41.03	22.08
		45	67.47	79.79	43.36	23.79
		50	72.59	83.28	46.30	25.86
		55	78.72	87.54	48.49	27.58
		60	84.90	91.54	50.75	28.96
		65	90.05	96.01	53.49	30.71
		70	94.15	98.81	56.42	32.22
		75	100.45	102.41	57.60	33.54
		80	101.99	105.76	60.20	34.56

Table 3-4. Continued.

Standing Height (cm)	Average Sitting Height (cm)	Weight (kg)	Waist Circumference (cm)	Average Buttocks Circumference (cm)	Thigh Circumference (cm)	Arm Circumference (cm)
		40	63.71	75.38	39.68	21.06
		45	65.35	78.92	41.58	22.79
		50	68.94	82.49	44.23	24.54
		55	71.86	85.56	47.00	26.46
		60	75.85	88.34	49.19	28.01
		65	80.40	92.03	51.60	29.68
165 cm	85.44	70	85.13	95.11	53.51	31.15
		75	90.71	99.27	55.49	32.12
		80	96.70	103.29	57.87	33.42
		85	99.39	105.50	59.48	34.81
		90	102.30	108.50	61.44	36.30
		95	108.00	111.61	62.81	36.38
		100	113.31	114.72	63.77	37.57
		105	115.51	117.83	67.72	39.98
		50	67.23	81.19	42.13	23.59
		55	69.52	85.50	44.73	25.45
		60	72.88	87.57	47.47	26.99
		65	75.45	90.46	49.72	28.46
		70	79.38	93.93	51.93	29.95
		75	83.26	96.70	54.06	31.39
		80	88.79	99.51	56.42	32.61
175 cm	89.80	85	92.86	103.97	57.75	33.65
		90	97.63	106.44	59.85	34.89
		95	102.09	107.77	61.45	36.38
		100	106.13	113.96	63.40	37.48
		105	109.57	114.91	64.93	38.14
		110	112.92	117.78	66.41	39.07
		115	116.51	120.65	67.34	40.82
		120	122.64	123.51	68.94	41.53
		125	124.13	126.38	71.02	42.31
		55	68.78	84.00	42.89	24.23
		60	71.74	87.09	46.00	25.84
		65	74.11	90.39	47.42	27.16
		70	77.27	92.41	50.49	28.85
		75	79.96	96.03	52.82	29.97
		80	83.19	99.15	54.78	31.32
		85	87.68	101.30	56.64	32.65
185 cm	95.58	90	91.35	104.26	58.46	34.17
		95	96.59	107.15	59.28	34.50
		100	101.34	110.05	61.42	36.13
		105	104.60	112.94	63.14	37.36
		110	108.13	115.84	63.91	37.99
		115	113.88	118.73	66.14	39.21
		120	116.32	121.62	68.72	40.36
		125	114.94	124.52	71.41	39.97

Table 3-5. Targeted heights, weight, and circumferential data for female pediatric phantoms.

Standing Height (cm)	Average Sitting Height (cm)	Weight (kg)	Waist Circumference (cm)	Average Buttocks Circumference (cm)	Thigh Circumference (cm)	Arm Circumference (cm)
85 cm	49.67	10	45.15	47.78	-	15.18
		15	49.47	52.02	-	16.56
95 cm	53.02	15	49.53	51.96	-	16.49
		20	57.62	60.61	-	19.41
105 cm	56.74	15	49.67	53.16	-	16.39
		20	54.17	57.71	-	18.10
		25	62.97	65.89	-	21.42
115 cm	60.96	20	52.96	58.02	-	17.58
		25	59.43	63.99	-	20.28
		30	66.63	71.84	-	22.53
125 cm	65.27	20	52.08	59.40	31.81	17.33
		25	56.26	63.91	34.89	18.99
		30	62.86	70.24	37.99	21.49
		35	71.07	76.00	42.26	23.81
		40	77.56	80.10	46.00	25.98
135 cm	69.56	25	55.19	64.08	34.26	18.34
		30	59.39	68.73	37.29	20.01
		35	66.62	74.58	40.95	22.52
		40	73.10	79.93	43.96	24.62
		45	77.61	86.04	46.20	26.37
		50	84.63	87.43	50.42	28.29
145 cm	74.95	30	58.58	69.86	35.78	19.27
		35	62.09	73.37	38.74	21.11
		40	67.22	78.60	42.21	23.02
		45	73.32	83.28	44.89	25.00
		50	78.47	88.27	47.25	26.70
		55	82.52	93.00	50.29	28.56
		60	87.60	96.05	52.65	30.05
		65	90.79	100.92	54.16	31.41
		70	94.15	105.05	57.76	32.30

Table 3-5. Continued.

Standing Height (cm)	Average Sitting Height (cm)	Weight (kg)	Waist Circumference (cm)	Average Buttocks Circumference (cm)	Thigh Circumference (cm)	Arm Circumference (cm)
		35	60.89	73.88	37.56	20.16
		40	65.35	78.19	40.54	21.97
		45	68.69	83.62	43.14	23.29
		50	72.16	87.81	46.12	25.10
		55	76.85	91.58	48.15	26.84
		60	81.88	95.35	50.74	28.24
155 cm	81.18	65	86.27	100.11	52.93	29.85
		70	91.98	102.97	54.71	31.11
		75	95.18	105.16	57.05	32.54
		80	99.02	109.44	60.31	34.14
		85	102.30	113.54	61.91	35.83
		90	105.09	117.35	63.07	36.87
		95	112.56	121.16	65.09	38.63
		40	62.77	77.82	38.79	20.24
		45	67.13	86.10	42.06	22.42
		50	70.18	87.28	44.61	23.93
		55	73.77	90.59	47.32	25.58
		60	78.18	94.88	49.62	26.99
		65	83.04	98.07	51.67	28.63
		70	86.54	101.78	54.13	30.07
165 cm	85.37	75	91.07	105.44	56.20	31.66
		80	96.16	107.79	57.84	32.76
		85	100.28	111.20	59.98	34.05
		90	102.89	115.10	62.08	35.90
		95	107.05	117.78	63.52	36.70
		100	108.28	121.46	65.93	38.60
		105	115.86	124.72	65.41	39.13
		110	119.43	127.97	69.26	40.29
		115	122.10	131.23	70.23	40.92
		50	68.80	86.56	42.78	22.95
		55	72.31	89.32	45.43	24.04
		60	75.20	95.34	48.38	25.92
		65	78.69	96.48	50.39	27.09
		70	82.53	100.65	52.61	28.29
		75	87.53	104.41	54.40	29.89
175 cm	89.41	80	92.16	106.54	56.13	31.39
		85	97.88	110.37	58.88	32.88
		90	99.19	113.69	60.16	34.26
		95	100.72	117.02	62.30	35.56
		100	106.08	120.35	65.13	37.01
		105	110.10	123.67	65.89	38.84
		110	113.93	127.00	67.86	39.32
		115	117.58	130.33	68.47	40.68

Table 3-6. Summary of organ doses for pediatric female phantoms at a fixed weight of 50 kg, at heights ranging from 135 cm to 175 cm, in 10 cm increments.

	Dose (mGy)				
Organ:	135 cm	145 cm	155 cm	165 cm	175 cm
Brain	0.22	0.22	0.16	0.15	0.14
Pituitary Gland	0.17	0.16	0.12	0.13	0.10
Lens	0.18	0.13	0.08	0.09	0.08
Eye balls	0.18	0.14	0.10	0.10	0.09
Salivary Glands	0.81	0.74	0.64	0.59	0.55
Oral Cavity layer	0.58	0.51	0.72	0.35	0.35
Spinal Cord	4.26	6.34	5.05	5.59	6.68
Thyroid	4.55	3.82	8.22	7.63	7.58
Esophagus	4.27	4.84	5.80	5.81	6.18
Trachea	4.46	5.00	5.98	5.82	6.22
Thymus	4.99	5.28	6.07	5.90	6.27
Lung	5.49	6.11	6.27	6.27	6.71
Breast	4.83	3.69	4.73	4.55	4.28
Heart Wall	5.62	5.42	6.11	6.22	6.10
Stomach Wall	5.20	5.76	6.05	6.86	6.63
Liver	6.06	5.82	6.92	5.80	7.16
Gall Bladder Wall	5.87	5.76	6.22	5.64	7.00
Adrenal	4.77	6.81	6.44	6.40	7.52
Spleen	4.96	6.24	5.55	8.64	7.06
Pancreas	4.81	6.16	5.83	6.96	7.27
Kidney	5.46	5.34	8.43	8.87	10.23
Small Intestine Wall	5.26	5.85	6.31	6.27	6.97
Colon Wall	5.92	6.06	6.57	6.61	7.21
Rectosigmoid Wall	4.74	5.21	5.07	5.27	5.41
Urinary Bladder Wall	5.48	5.01	5.24	5.04	5.66
Uterus	4.44	4.63	4.61	4.38	4.95
Ovaries	4.84	5.13	5.05	5.08	5.41
Skin	3.13	2.85	3.16	3.25	3.35
Residual soft tissue (muscle)	3.45	3.58	3.50	4.03	4.03

Table 3-7. Summary of organ doses for pediatric female phantoms at a fixed height of 165 cm, at weights ranging from 40 kg to 115 kg.

	Dose (mGy)															
Organ:	40 kg	45 kg	50 kg	55 kg	60 kg	65 kg	70 kg	75 kg	80 kg	85 kg	90 kg	95 kg	100 kg	105 kg	110 kg	115 kg
Brain	0.14	0.14	0.15	0.14	0.14	0.15	0.15	0.15	0.15	0.15	0.15	0.15	0.15	0.15	0.15	0.14
Pituitary Gland	0.12	0.13	0.13	0.12	0.13	0.13	0.14	0.13	0.14	0.12	0.14	0.15	0.13	0.13	0.12	0.15
Lens	0.08	0.09	0.09	0.10	0.09	0.10	0.10	0.08	0.10	0.10	0.11	0.10	0.11	0.11	0.12	0.13
Eye balls	0.10	0.10	0.10	0.10	0.10	0.10	0.10	0.11	0.11	0.11	0.11	0.13	0.11	0.12	0.12	0.13
Salivary Glands	0.58	0.58	0.59	0.59	0.63	0.64	0.65	0.64	0.65	0.64	0.63	0.64	0.60	0.58	0.58	0.59
Oral Cavity layer	0.36	0.35	0.35	0.37	0.41	0.38	0.41	0.40	0.41	0.40	0.40	0.41	0.39	0.36	0.37	0.37
Spinal Cord	6.07	6.05	5.59	5.33	5.07	4.76	4.55	4.37	4.06	3.59	3.82	3.23	3.48	3.18	3.24	2.90
Thyroid	8.26	7.98	7.63	7.60	7.45	7.26	7.10	7.05	7.10	6.38	6.12	5.20	5.51	4.59	4.61	4.38
Esophagus	6.41	6.28	5.81	5.54	5.31	4.95	4.73	4.60	4.43	4.03	4.13	3.46	3.84	3.44	3.54	3.28
Trachea	6.38	6.25	5.82	5.76	5.41	5.17	5.06	4.94	4.88	4.54	4.61	3.90	4.39	3.82	3.88	3.59
Thymus	6.47	6.30	5.90	5.84	5.41	5.23	5.06	4.99	4.90	4.65	4.67	3.97	4.47	3.94	3.96	3.67
Lung	6.91	6.74	6.27	5.99	5.65	5.37	5.07	4.94	4.76	4.47	4.47	3.95	4.24	3.92	3.97	3.67
Breast	5.21	4.75	4.55	4.26	4.03	3.98	3.62	3.48	3.37	3.13	2.94	2.82	2.90	2.69	2.65	2.44
Heart Wall	6.97	6.65	6.22	5.88	5.53	5.33	4.89	4.75	4.57	4.24	4.14	3.73	3.93	3.63	3.62	3.36
Stomach Wall	8.03	7.23	6.86	6.67	6.31	5.88	5.63	5.17	5.31	4.50	4.48	4.12	4.10	3.85	3.80	3.59
Liver	6.86	6.27	5.80	5.58	5.23	4.81	4.56	4.26	4.07	3.57	3.58	3.17	3.17	2.92	2.95	2.69
Gall Bladder Wall	6.84	6.09	5.64	5.48	5.10	4.61	4.45	4.19	3.95	3.41	3.46	3.07	3.07	2.83	2.78	2.56
Adrenal	7.16	6.85	6.40	6.18	5.72	5.43	5.27	5.05	4.71	3.93	4.22	3.66	3.77	3.54	3.57	3.22
Spleen	9.32	8.93	8.64	8.42	8.05	7.91	7.73	7.22	7.48	6.02	6.43	5.56	5.79	5.67	5.75	5.34
Pancreas	7.86	7.38	6.96	6.76	6.30	5.98	5.90	5.42	5.32	4.46	4.62	4.14	4.17	3.95	3.89	3.57
Kidney	9.36	9.36	8.87	8.65	8.10	7.87	7.61	7.22	6.62	5.81	6.07	5.50	5.51	5.18	5.07	4.54
Small Intestine Wall	7.19	6.50	6.27	5.94	5.46	5.05	4.84	4.37	4.06	3.73	3.55	3.30	3.21	2.91	2.74	2.58
Colon Wall	7.57	6.85	6.61	6.28	5.87	5.43	5.32	4.76	4.47	4.13	3.88	3.65	3.56	3.22	3.03	2.91
Rectosigmoid Wall	6.03	5.37	5.27	5.05	4.58	4.37	4.01	3.74	3.51	3.28	3.01	2.91	2.69	2.56	2.36	2.19
Urinary Bladder Wall	6.11	5.27	5.04	4.77	4.59	4.48	4.03	3.74	3.52	3.34	2.95	2.98	2.57	2.40	2.09	2.02
Uterus	5.22	4.59	4.38	4.16	3.84	3.76	3.35	3.17	2.93	2.77	2.48	2.46	2.16	2.07	1.85	1.75
Ovaries	6.03	5.24	5.08	4.80	4.44	4.24	3.88	3.58	3.36	3.20	2.94	2.85	2.55	2.41	2.19	2.07
Skin	3.49	3.39	3.25	3.13	2.99	2.88	2.78	2.73	2.63	2.59	2.54	2.48	2.44	2.39	2.34	2.31
Residual soft tissue (muscle)	4.25	4.35	4.03	3.79	3.45	3.34	3.24	3.26	3.01	3.04	2.96	2.92	2.73	2.73	2.63	2.56

Table 3-8. Percent difference between interpolated and Monte Carlo calculated organ doses for 165 cm phantoms, removing every other phantom (10 kg intervals).

	% Diff														
Organ	40 kg	45 kg	50 kg	55 kg	60 kg	65 kg	70 kg	75 kg	80 kg	85 kg	90 kg	95 kg	100 kg	105 kg	110 kg	115 kg
Thymus	-	-4.08	-	-2.84	-	0.20		-2.72	-	-3.48	-	6.58	-	-2.77	-	-2.18
Lung	-	-1.66	-	0.62	-	2.52	-	3.60	-	5.45	-	16.41	-	12.78	-	16.64
Breast	-	1.47	-	1.16	-	-5.80	-	-4.41	-	-1.59	-	-0.69	-	-3.01	-	1.36
Heart W	-	-0.54	-	1.72	-	1.38	-	4.41	-	7.46	-	18.34	-	15.23	-	21.13
Stomach W	-	2.01	-	-1.74	-	-0.19	-	-1.84	-	-0.51	-	-2.57	-	-6.03	-	-8.18
Liver	-	2.42	-	0.85	-	1.80	-	4.95	-	9.20	-	11.00	-	9.98	-	9.38
Gall Bladder W	-	2.99	-	1.88	-	4.26	-	5.33	-	13.59	-	12.88	-	12.79	-	15.31
Adrenal	-	-1.61	-	-1.69	-	0.76	-	-1.02	-	10.08	-	6.73	-	2.23	-	4.58
Spleen	-	-1.06	-	-2.29	-	-0.24	-	-1.25	-	7.15	-	7.46	-	0.65	-	1.85
Pancreas	-	0.21	-	-1.01	-	1.88	-	1.62	-	9.55	-	5.82	-	5.06	-	8.03
Kidney	-	-3.11	-	-2.91	-	-1.66	-	-1.53	-	7.51	-	1.29	-	-1.33	-	0.10
SI W	-	3.19	-	0.67	-	1.70	-	2.28	-	3.91	-	1.64	-	2.43	-	2.31
Colon W	-	4.39	-	2.42	-	3.58	-	4.91	-	6.68	-	6.46	-	9.03	-	8.70
Rectosigmoid W	-	6.32	-	1.26	-	0.94	-	3.29	-	3.43	-	3.38	-	9.69	-	18.49
Urinary bladder W	-	5.62	-	4.15	-	-6.08	-	-4.23	-	-10.00	-	-16.25	-	-13.72	-	-18.79
Uterus	-	6.07	-	2.72	-	-2.23	-	0.91	-	-1.53	-	-3.07	-	4.67	-	10.44
Ovaries	-	6.97	-	4.52	-	1.13	-	5.54	-	5.57	-	4.12	-	12.43	-	19.95

Table 3-9. Percent difference between interpolated and Monte Carlo calculated organ doses for 165 cm phantoms, at 15 kg intervals

	% Diff															
Organ	40 kg	45 kg	50 kg	55 kg	60 kg	65 kg	70 kg	75 kg	80 kg	85 kg	90 kg	95 kg	100 kg	105 kg	110 kg	115 kg
Thymus	-	-1.99	1.51	-	3.63	3.76	-	1.30	-1.53	-	-3.70	11.93	-	2.35	-1.16	-
Lung	-	-3.37	-1.58	-	-0.89	-1.37	-	-2.39	-3.43	-	-6.67	2.49	-	-5.34	-10.57	-
Breast	-	1.23	-0.39	-	-0.06	-4.73	-	-3.06	-3.30	-	-0.09	-0.10	-	-3.71	-7.42	-
Heart W	-	-0.77	0.78	-	2.73	1.47	-	4.24	4.25	-	5.04	16.23	-	11.55	8.17	-
Stomach W	-	3.76	3.28	-	-1.38	0.51	-	-1.40	-6.23	-	-6.18	-1.64	-	-4.17	-7.70	-
Liver	-	1.98	1.55	-	-2.61	-2.51	-	-1.54	-6.34	-	-4.77	-0.13	-	-2.99	-6.98	-
Gall Bladder W	-	2.67	3.04	-	-2.36	-0.75	-	-2.26	-5.84	-	-4.96	-0.72	-	-3.35	-5.92	-
Adrenal	-	-0.55	0.74	-	0.40	-0.24	-	-2.90	-3.66	-	-3.65	3.40	-	-1.10	-3.95	-
Spleen	-	0.32	1.25	-	0.67	-1.19	-	-3.29	-5.93	-	-7.49	3.32	-	-3.67	-6.88	-
Pancreas	-	1.98	3.43	-	2.28	2.58	-	2.01	0.53	-	1.58	6.51	-	6.53	5.82	-
Kidney	-	-1.53	0.17	-	1.80	0.39	-	1.11	3.56	-	2.92	6.31	-	5.40	4.40	-
SI W	-	2.33	-0.47	-	-1.88	-1.15	-	-1.95	-3.07	-	-4.95	-6.22	-	-7.92	-8.19	-
Colon W	-	2.87	0.09	-	-2.14	-0.78	-	-1.38	-2.46	-	-3.40	-4.86	-	-5.81	-5.79	-
Rectosigmoid W	-	7.76	4.44	-	5.08	3.26	-	6.30	6.32	-	10.05	8.03	-	15.61	22.01	-
Urinary bladder W	-	6.47	4.69	-	-0.73	-4.99	-	-2.31	-4.05	-	-1.85	-10.90	-	-4.19	3.33	-
Uterus	-	6.99	5.04	-	2.86	-1.24	-	2.00	1.17	-	4.08	-1.89	-	6.01	11.35	-
Ovaries	-	5.93	2.58	-	0.27	-2.72	-	-0.49	-2.44	-	-2.38	-7.07	-	-3.17	2.25	-

Table 3-10. Percent difference between interpolated and Monte Carlo calculated organ doses for 165 cm phantoms, at 20 kg intervals

	% Diff															
Organ	40 kg	45 kg	50 kg	55 kg	60 kg	65 kg	70 kg	75 kg	80 kg	85 kg	90 kg	95 kg	100 kg	105 kg	110 kg	115 kg
Thymus	-	-1.96	0.94	-0.95	-	2.98	2.12	2.06	-	4.87	2.14	21.81	-	18.85	19.38	30.01
Lung	-	-1.73	0.26	0.33	-	2.24	3.74	3.63	-	6.13	4.99	18.29	-	16.08	13.54	21.94
Breast	-	1.69	-0.44	1.27	-	-5.47	-2.03	-3.41	-	0.70	2.08	3.56	-	3.78	2.27	11.96
Heart W	-	-2.33	-1.56	-1.37	-	-3.16	-0.82	-1.96	-	-0.99	-2.99	6.88	-	2.01	-1.16	5.27
Stomach W	-	4.82	4.95	1.66	-	4.37	2.69	4.32	-	8.15	2.75	9.15	-	9.39	6.91	11.92
Liver	-	2.66	3.27	1.14	-	1.68	2.28	3.83	-	6.28	0.82	5.40	-	0.89	-4.44	-4.21
Gall Bladder W	-	2.80	3.84	0.70	-	1.60	-0.44	0.67	-	5.81	-2.21	1.74	-	-2.45	-6.16	-5.16
Adrenal	-	-1.20	0.71	-1.11	-	1.57	0.60	0.01	-	11.52	0.68	8.45	-	4.21	1.30	6.97
Spleen	-	0.42	2.06	-0.50	-	2.24	2.67	2.29	-	12.74	1.88	15.51	-	11.18	9.25	16.25
Pancreas	-	0.92	2.42	-0.75	-	1.87	0.17	1.58	-	9.84	1.70	6.87	-	7.41	6.97	12.41
Kidney	-	-3.14	-1.43	-2.75	-	-1.07	-1.35	-0.24	-	10.08	1.81	5.26	-	4.60	3.75	8.91
SI W	-	2.72	-0.09	-0.64	-	-0.42	-2.68	-0.55	-	0.53	-1.59	-1.88	-	-0.90	0.64	-0.20
Colon W	-	3.73	0.97	0.63	-	0.63	-2.26	0.81	-	1.47	0.86	0.38	-	2.13	3.95	1.49
Rectosigmoid W	-	5.05	0.78	-1.70	-	-4.23	-3.18	-4.84	-	-8.20	-8.16	-12.35	-	-11.91	-10.15	-10.43
Urinary bladder W	-	7.73	5.57	5.48	-	-5.43	-2.26	-3.93	-	-9.76	-5.94	-15.59	-	-11.82	-6.62	-14.51
Uterus	-	5.60	2.78	0.46	-	-6.58	-3.86	-6.47	-	-12.26	-10.50	-17.89	-	-16.77	-15.74	-18.67
Ovaries	-	8.03	4.87	4.83	-	0.88	4.18	4.97	-	5.06	7.38	4.21	-	13.90	23.79	23.92

Table 3-11. Percent difference between interpolated and Monte Carlo calculated organ doses for 165 cm phantoms, at 25 kg intervals.

	% Diff															
	40 kg	45 kg	50 kg	55 kg	60 kg	65 kg	70 kg	75 kg	80 kg	85 kg	90 kg	95 kg	100 kg	105 kg	110 kg	115 kg
Thymus	-	-2.05	1.50	-0.01	3.69	-	2.38	1.36	-1.50	0.99	-	11.75	-7.41	1.93	-1.72	-
Lung	-	-2.10	0.23	0.48	2.09	-	3.35	2.60	2.29	3.02	-	11.36	-1.24	4.84	0.04	-
Breast	-	4.97	3.86	6.69	5.50	-	5.63	4.64	5.26	9.45	-	11.81	2.60	9.99	6.87	-
Heart W	-	-0.27	1.53	2.71	3.84	-	5.93	5.39	5.24	7.38	-	16.10	3.39	10.01	5.80	-
Stomach W	-	4.51	4.47	1.01	0.76	-	1.37	2.71	-1.55	5.86	-	6.14	0.02	5.61	2.84	-
Liver	-	2.58	2.80	0.37	-0.16	-	1.16	2.82	-1.62	5.95	-	6.53	2.54	4.30	0.30	-
Gall Bladder W	-	2.37	3.06	-0.36	-1.81	-	-2.18	-1.22	-4.79	3.74	-	0.01	-5.31	-3.41	-6.55	-
Adrenal	-	-2.10	-0.44	-2.54	-0.26	-	-2.35	-3.64	-4.74	5.39	-	-0.15	-7.12	-7.25	-11.65	-
Spleen	-	-0.25	1.38	-1.29	2.09	-	0.55	-0.64	-3.17	6.92	-	5.76	-4.80	-2.98	-7.40	-
Pancreas	-	1.20	2.92	-0.11	2.24	-	0.98	2.31	0.80	10.10	-	6.11	1.50	5.05	3.61	-
Kidney	-	-3.16	-1.16	-2.29	0.84	-	-0.92	-0.07	2.00	9.14	-	2.51	-1.18	-0.93	-3.50	-
SI W	-	3.81	1.38	1.28	1.06	-	0.88	3.78	3.90	6.54	-	5.92	4.86	9.28	12.26	-
Colon W	-	3.33	0.45	-0.04	-1.82	-	-3.45	-0.64	-1.42	-0.51	-	-2.19	-4.42	-1.21	0.13	-
Rectosigmoid W	-	5.84	1.90	-0.29	0.62	-	-1.17	-2.83	-4.93	-6.60	-	-11.89	-10.68	-13.62	-13.52	-
Urinary bladder W	-	10.78	9.41	10.29	4.85	-	5.65	5.31	4.30	2.30	-	-0.09	10.44	10.39	20.96	-
Uterus	-	6.64	4.18	2.19	0.54	-	-1.56	-4.21	-6.87	-10.52	-	-17.41	-14.32	-18.71	-19.60	-
Ovaries	-	6.26	2.74	2.09	-0.18	-	-1.90	-2.93	-5.88	-7.62	-	-14.93	-13.27	-16.34	-14.99	-

CHAPTER 3
CONCLUSION AND FUTURE WORK

As a result of increasing obesity trends in the United States among pediatrics, an expansion of the current UF/NCI family of reference hybrid phantoms was necessary. The updated grid-based library will serve as a comprehensive pediatric library reflecting the most current anthropometric data provided by the CDC. The work presented in this study has been extended to adult male and female populations in the United States, and coupled with the pediatric library, will serve as a useful tool for radiation protection and organ dosimetry purposes. Including the adult male and female library, a total of 358 NURBS phantoms will be created. This is made possible due to the relative ease in which NURBS surfaces can be molded, with the phantom scaling process taking 30 minutes to complete. In the future, these NURBS and polygon mesh based phantoms will be used with MCNPX to create a pre-computed dose library for CT examinations that will ultimately be implemented into patient dose-tracking programs. Due to large computational run-times, interpolation of organ doses using the methods presented in this study will be imperative to completing a pre-computed dose library for CT examinations.

In addition to CT applications, the extended adult and pediatric libraries can be used in a variety of modalities, including fluoroscopy and nuclear medicine. In fluoroscopy, the reference point air KERMA can be translated to the location of a patient's skin using patient-dependent phantoms using skin dose mapping to visually monitor skin dose during interventional fluoroscopy procedures. Implementing skin dose mapping in the future in real-time would allow physicians to modify behavior when skin doses approach levels associated with deterministic risks of radiation. Many patients

undergoing interventional fluoroscopic procedures deviate significantly from 50th percentile reference weight values, making the availability of a comprehensive library of patient-dependent computational models crucial for accurate dose assessments.

In addition to their applications in radiation protection and dosimetry studies, the library of patient-dependent phantoms can be used in the future to further increase the specificity of phantom modeling on a patient-by-patient basis. Through internal organ sculpting, a closest-matched patient-dependent phantom chosen from the extended library can be altered to create a patient-sculpted phantom unique to an individual when increased accuracy is needed. Though this sculpting process can be done manually, the possibility of automation through the use of Rhinoceros script language can be explored in the future to expedite the sculpting process.

APPENDIX
COMPUTED TOMOGRAPHY MODELING AND SIMULATION

The following write-up was provided by Daniel Long (MS Student-Medical Physics, ALRADS) from the University of Florida for the CT portion of the simulation.

Computed Tomography Scanner Description

A SOMATOM Sensation 16 multi-detector CT scanner (Siemens Medical Solutions, Erlangen, Germany) was used as the basis for the Monte Carlo source term as well as used for all physical dose measurements. The scanner contained 16 rows of detectors that allowed beam collimations from 10-24 mm, had the ability to scan in both axial and variable-pitch helical modes, and featured two settings of inherent filtration for head and body scanning along with a single bowtie beam-shaping filter. The fan beam angle was 52°, with a focal-spot-to-isocenter distance of 57 cm. The operator could select tube potentials of 80, 100, 120, or 140 kVp along with varying tube current and gantry rotation speeds. The scanner also allowed for use of tube-current modulation during scanning, but this feature was not used for the measurements in this study.

Modeling of the Computed Tomography Scanner X-ray Source

The source term of the scanner was created as a custom source file within a general-purpose Monte Carlo radiation transport code, MCNPX2.6.23. Material and thickness of the two inherent filters for head and body scanning was obtained from the manufacturer. This information, in conjunction with a commercial spectrum generation program, SPEC78 (Institute of Physics and Engineering in Medicine), was used to create x-ray spectra for the head and body filters for all beam energies.[11] These spectra were incorporated into the MCNPX source term through an input deck for energy sampling. To account for the effects of the bowtie filter on the shape of the fan beam for all beam

energy/filter combinations, angular-dependent weighting factors were applied in the source term based on free-in-air lateral dose profile measurements made previously by 14 a pencil ion chamber while the x-ray tube was fixed at the 12 o'clock position in service mode.[12] The effects of overbeaming on the true beam thicknesses for various collimation settings were previously quantified in studies using radiographic film, and were thus taken into account within the source term.[13]

The custom source term allowed the user to simulate both axial exams and helical exams with varying pitch. For helical exams, this was accomplished by having the source first sample the location of the x-ray focal spot along a mathematically-described helix based on the pitch and scan length selected by the user as well as the previously-defined focal-spot-to-isocenter distance of 57 cm. For axial exams, the focal spot location would be sampled along a series of circular rings of radius 57 cm spanning the total specified length of the scan that were spaced apart by the distance of the beam collimation selected. After selecting this starting location of the x-ray focal spot, the source sampled an angle within the 52° fan beam as well as within the beam collimation thickness, therefore selecting a directional path upon which the photon would initially travel. Finally, the photon energy was sampled based on the energy spectrum selected for the exam. This process would be repeated for the total number of particles to be transported as selected by the user. The final version of the source term allowed the user to select beam energy, head or body filtration, beam collimation, an axial or a helical exam with associated pitch, and starting angle of the beam for helical exams.

Computational Phantom Dose Measurements

Organ dose calculations using the Monte Carlo CT source term were performed using 20 hybrid computation phantoms. The phantoms were voxelized to resolutions of

3 x 3 x 3 mm^3 (adult and 15-year-old phantoms) 2 x 2 x 2 mm^3 (10-year-old phantom) for input into MCNPX for dose calculations. Within the Monte Carlo simulation setups, the voxelized phantoms were placed upon a model of the scanner's carbon-fiber patient table. The table was modeled as two concentric cylinders of different radii that were truncated to a width of 40 cm corresponding to the width of the patient table, with carbon fiber as its material composition. The source term was then set up to reflect the parameters of each physical scan. For all helical scans, the beam starting angle was assumed to be 0°. Organ doses were then calculated using the F6 KERMA approximation tally in MCNPX; therefore, no secondary electrons were transported in the calculation. Considering the energy range of the CT x-ray spectra and the subsequent ranges of secondary electrons in tissue, the KERMA approximation offers an acceptably accurate approximation of average organ dose. For all computational calculations, 100 million particles were transported.

Since MCNPX provides calculation results in dose per simulated photon, the number of photons delivered by the scanner per unit mAs, called the Monte Carlo normalization factor, were multiplied to the MCNPX dose results to obtain organ doses in absolute units. The normalization factors were calculated based on the ratio of pencil ion chamber measurements in free-in-air (mGy/mAs) to MCNPX-simulated free-in-air ion chamber doses (mGy/photon) made in previous studies.[12] Absolute organ doses for each individual scan could then be calculated by multiplying the dose in mGy/mAs by the total mAs delivered during the exam.

LIST OF REFERENCES

1H. Hricak, D. J. Brenner, S. J. Adelstein, D. P. Frush, E. J. Hall, R. W. Howell, C. H. McCollough, F. A. Mettler, M. S. Pearce, O. H. Suleiman, J. H. Thrall, and L. K. Wagner, “Managing Radiation Use in Medical Imaging: A Multifaceted Challenge,” Radiology 258, 889-905 (2011)

[2]NCRP, NCRP Report No. 160: *Ionizing Radiation Exposure of the Population of the United States*, NCRP Report No. 160. (National Council on Radiation Protection and Measurement, Bethesda, MD, 2009)

[3]D. Broggio, J. Beurrier, M. Bremaud, A. Desbrée, J. Farah, C. Huet, and D. Franck, “Construction of an Extended Library of Adult Male 3D Models: Rationale and Results,” Physics in Medicine and Biology **56**, 7659-7692 (2011)

[4]Y. H. Na, B. Zhang, J. Zhang, P. F. Caracappa, and X. G. Xu, “Deformable Adult Human Phantoms for Radiation Protection Dosimetry: Anthropometric Data Representing Size Distributions of Adult Worker Populations and Software Algorithms,” Physics in Medicine and Biology **55**, 3789-3811 (2010)

[5]V. F. Cassola, F. M. Milian, R. Kramer, C. A. B. de Oliveira Lira, and H. J. Khoury, “Standing Adult Human Phantoms Based on 10^{th}, 50^{th}, and 90^{th} Mass and Height Percentiles of Male and Female Caucasian Populations,” Physics in Medicine and Biology **56**, 3749-3772 (2011)

[6]V. F. Cassola, V. J. de Milo Lima, R. Kramer, H. J. Khoury, “FASH and MASH: Female and Male Adult Human Phantoms Based on Polygon Mesh Surfaces: Part I. Development of Anatomy,” Physics in Medicine and Biology **55,** 4399-4430 (2010)

[7]G. L. De la Grandmaison, I. Clairand, and M. Durigon, “Organ Weight in 684 Adult Atopsies: New Tables for a Caucasoid Population,” Forensic Science International **119**, 149-154

[8]C. Lee, D. Lodwick, J. Hurtado, D. Pafundi, J. L. Williams, and W. Bolch, “The UF Family of Reference Hybrid Phantoms for Computational Radiation Dosimetry,” Physics in Medicine and Biology **55**, 339-363 (2010)

[9]P. Johnson, S. R. Whalen, M. Wayson, B. Juneja, C. Lee, and W. E. Bolch, “Hybrid Patient-Dependent Phantoms Covering Statistical Distributions of Body Morphometry in the U.S. Adult and Pediatric Populations,” Proceedings of IEEE **97**, 2060-2075 (2009)

[10]Centers for Disease Control and Prevention (2011, April 21, 2011). "Overweight and Obesity." Data and Statistics. Retrieved December 12, 2011, from http://www.cdc.gov/obesity/childhood/data.html.

[11]K. Cranley, B. Gilmore, G. Fogarty, and L. Desponds, “IPEM report 78: Catalogue of diagnostic X-ray spectra and other data,” York: The Institute of Physics and Engineering in Medicine (1997).

[12]C. Lee, K.P. Kim, D. Long, R. Fisher, C. Tien, S.L. Simon, A. Bouville, W.E. Bolch, “Organ doses for reference adult male and female undergoing computer tomography estimated by Monte Carlo simulations,” Medical Physics **38**, 1196-1206 (2011).

[13]R. J. Staton, C. Lee, C. Lee, M. D. Williams, D. E. Hintenlang, M. M. Arreola, J. L. Williams, and W. E. Bolch, “Organ and effective doses in newborn patients during helical multislice computerd tomography examination,” Physics in Medicine and Biology **51**, 5151-5166 (2006).

BIOGRAPHICAL SKETCH

Amy Marie Geyer was born in Newport Beach, California to Bill and Pat Geyer. After spending the majority of her childhood living in Idaho, she attended a sports academy in Bradenton, Florida and graduated high school from The Pendleton School in 2004. She graduated with her Bachelor of Science in nuclear engineering sciences from the University of Florida in May 2010 and graduated with her Master of Science in biomedical engineering with a specialty in medical physics from the University of Florida in May 2012. Upon graduation, she began pursuing her Doctorate of Philosophy in the same field.